Unsupervised Clustering for Identifying Dusty Days and Their Sources: A Long-Term Data Study in Sanandaj, Iran

Mohammad Momen Haji Mirzaei[1*], Yashar Mohammadi[2]

[1]: M.Sc. in Environmental Engineering, School of Engineering, Civil Engineering Department; Urmia University, Iran. Email address: momenhajimirzay@gmail.com.

[2]: M.Sc. in Environmental Engineering, School of Engineering, Civil Engineering Department; Urmia University, Iran. Email address: y.mohammadi@urmia.ac.ir.

[*]: Corresponding Author: Mohammad Momen Haji Mirzaei. km 11, University Boulevard (Urmia-Sero Road), School of Engineering, Civil Engineering Department, Urmia University, Urmia, Iran. Email: momenhajimirzay@gmail.com. Phone: +98 (0) 936 999 7620.

Fax: +98 (0) 441 275 274 0 to 4.

Unsupervised Clustering for Identifying Dusty Days and Their Sources: A Long-Term Data Study in Sanandaj, Iran

Abstract

Dust storms are a persistent environmental hazard in the Middle East, yet long-term monitoring remains limited by sparse ground observations and the lack of objective, reproducible event definitions. This study develops a transferable, data-driven framework for objectively identifying dusty days in data-scarce regions and explicitly addresses two key issues: defining dust events using defensible multi-indicator criteria instead of arbitrary thresholds, and linking objectively detected events to dominant dust source regions. Long-term PM_{10} records were combined with satellite and reanalysis aerosol indices, including Aerosol Optical Depth at 550 nm (AOD_{550}), Dust Optical Depth (DOD), and Dust Aerosol Optical Depth ($DUAOD_{550}$) from CAMS and MERRA-2. Quantitative thresholds derived using statistical analyses and K-Means clustering produced physically consistent criteria ($PM_{10} \geq 75$ μg m^{-3}; $AOD_{550} \geq 0.45$; DOD ≥ 0.20; $DUAOD_{550} \geq 0.20$), capturing the episodic, right-skewed nature of dust variability. Among Boolean rules, OR logic provided the most comprehensive detection (616 dusty days) and remained robust under ±2% perturbations, while Meteorological Aerodrome Reports (METAR) dust and visibility codes confirmed higher recall than restrictive schemes. Using these objectively identified events, 72-h Hybrid Single-Particle Lagrangian Integrated Trajectory (HYSPLIT) backward trajectories with resampling, Principal Component Analysis (PCA), and K-Means clustering revealed two distinct regimes: regional transport from the Iraq-Iran borderlands and southern Mesopotamia, and longer-range intrusions from the Syrian Desert and northern-western Mesopotamia. Unlike previous single-indicator studies, this work provides a unified framework integrating objective thresholding, independent validation, and trajectory source attribution, supporting scalable monitoring, early warning, and risk management in arid and semi-arid regions.

Keywords: Dust storms, Unsupervised machine learning, Trajectory clustering, Satellite remote sensing, Transboundary air pollution.

1. Introduction

Dust storms are widely recognized as a major environmental challenge driven by complex climatic, environmental, and anthropogenic interactions. Their frequency and intensity have increased in recent decades due to extensive land degradation and desertification in arid and semi-arid regions, with nearly 46% of the Earth's surface and more than 500 million people directly affected (IPCC, 2019). Climate change, through alterations in precipitation, wind regimes, and soil properties, has further enhanced the potential for dust emissions, making the Middle East and North Africa among the most vulnerable regions (World Bank, 2019). Beyond their environmental implications, dust storms significantly deteriorate air quality, elevating PM_{10} and $PM_{2.5}$ concentrations to levels associated with increased respiratory and cardiovascular mortality (Papatheodorou & Achilleos, 2025). According to the World Health Organization, air pollution contributes to nearly seven million premature deaths annually, with mineral dust being a major contributor in arid regions (WHO, 2021). Dust also imposes considerable economic impacts, disrupting transportation, damaging renewable energy infrastructure, reducing agricultural productivity, and increasing food production costs (UNEP, 2016). Moreover, dust induced radiative perturbations can influence regional climate and potentially suppress precipitation (Parajuli et al., 2022). These wide ranging impacts have prompted international organizations such as UNEP and WMO to emphasize the development of improved monitoring frameworks, early warning systems, and coordinated regional management strategies.

Sanandaj, located in western Iran and downwind of major dust source regions in Iraq and Syria, has experienced a marked escalation in dust frequency and severity over the past two decades (Shahabi et al., 2023). This situation underscores the need for reliable, locally tailored approaches for dusty day detection and source attribution. However, existing studies reveal several methodological challenges. A key limitation concerns the absence of a consistent and objective definition of "dust days." Many studies rely on simple single threshold surface criteria such as $PM_{10} > 150$ µg/m³ (Shahsavani et al., 2020), which, although practical, fail to fully represent the spatiotemporal variability and atmospheric transport dynamics of dust events. Alternative indicators ($PM_{2.5}/PM_{10}$ ratios) and satellite based metrics such as Aerosol Optical Depth (AOD) have been widely examined, yet their reliability varies across space, time, and meteorological conditions (Fan et al., 2021; Yang et al., 2019; Labban & Butt, 2023). Newly developed indices such as Brightness Temperature Difference (BTD) and Normalized Difference Dust Index (NDDI) also remain largely empirical and region dependent (Yang et al., 2023). Even in machine learning applications, many approaches continue to rely on health based thresholds, PM_{10} > 50 µg/m³ (Safarian et al., 2025), which are suitable for risk communication but not necessarily optimal for objectively identifying dust episodes. Previous studies have greatly advanced understanding of Middle Eastern dust dynamics, but variations in event definitions, reliance on single indicators, and heterogeneous datasets complicate comparison and limit transferability. This highlights the need for a reproducible, data-driven framework that integrates multiple indicators and objectively links event identification to sources.

Trajectory modeling provides an essential basis for understanding dust transport mechanisms. The HYSPLIT model has been widely applied to simulate backward and forward trajectories and, when combined with satellite products, has proven effective in identifying dominant source regions over extended spatial domains (Borna et al., 2021). Numerous studies have demonstrated its robustness (Iraji et al., 2021; White et al., 2023); however, trajectory interpretation frequently relies on manual or qualitative assessments, introducing subjectivity and limiting systematic long-term evaluations. Clustering and machine learning techniques offer an opportunity to extract objective and reproducible structure from complex trajectory ensembles, yet comprehensive long-term applications at the city scale remain scarce, particularly for Sanandaj. Most existing works in the region have addressed individual aspects such as PM health impacts (Ebrahimi et al., 2014), chemical composition (Hosseini et al., 2015), MODIS AOD assessments (Amanollahi et al., 2011), or microbial air loads (Nourmoradi et al., 2015), without establishing an integrated framework for dust identification and transport analysis.

Accordingly, this study is designed to address two closely related scientific questions: how dusty days can be objectively defined using defensible, multi indicator criteria rather than arbitrary single thresholds, particularly in data scarce environments, and how these objectively detected events relate to dominant dust source regions and transport regimes. To this end, we develop a unified and transferable framework that derives quantitative dust event thresholds from long term, ground-based PM_{10} observations integrated with satellite and reanalysis aerosol indices through statistical analysis and unsupervised clustering. The identified events are then rigorously validated against independent METAR dust and visibility observations, ensuring robustness and reproducibility. Finally, objectively defined dusty days are linked to physically meaningful source regions using 72-h HYSPLIT backward trajectories combined with trajectory resampling, principal component analysis, and clustering. Unlike previous studies that rely on single indicators, arbitrary cutoffs, or qualitative trajectory interpretation, this work provides a fully integrated framework that combines objective thresholding, independent validation, and trajectory source attribution. As such, the proposed approach offers a scalable and transferable basis for long-term dust monitoring and risk assessment in arid and semi-arid regions.

2. Methods and Materials

2-1. Study Area

Sanandaj, the capital of Kurdistan Province in western Iran (35.31°N, 46.99°E), is located at an elevation of 1,521 m above sea level and hosts a population of over 412,000 inhabitants (Statistical Center of Iran, 2018). The city lies on the foothills of the Zagros Mountains within the Middle East dust belt (Figure 1), where complex topography influences regional airflow and favors dust intrusions. According to the Köppen climate classification, Sanandaj experiences a cold semi-arid climate (BSk), characterized by hot, dry summers and cold winters (Modarres & Sarhadi, 2009). Its environmental setting, including light soils and sparse steppe vegetation, makes the region highly susceptible to dust activity, the frequency

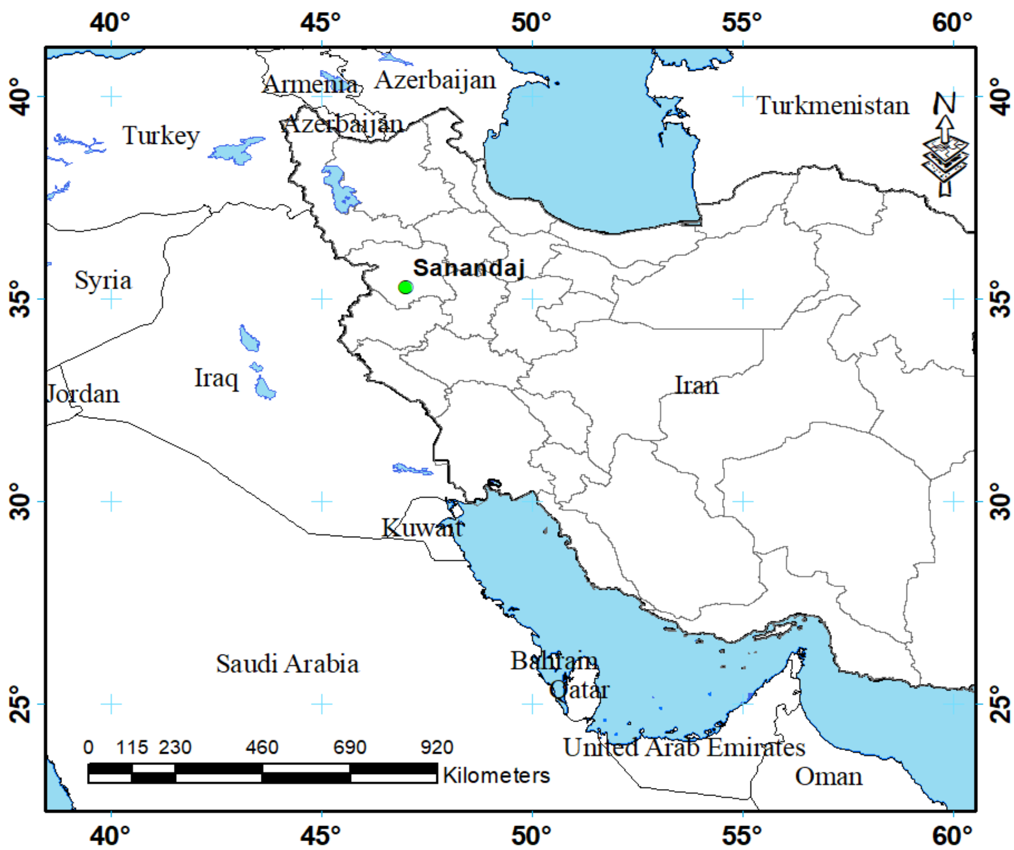

Figure 1. Geographical location of the study area (Sanandaj, western Iran).

and intensity of which have increased markedly over the past two decades (Abadi et al., 2025).

2–2. Computational Environment and Tools

All data processing and analyses were performed using Python-based workflows. Backward air-mass trajectories were generated using the HYSPLIT model via the NOAA READY system for all identified dusty days and subsequently processed for statistical analysis and clustering. The overall computational workflow was designed to ensure full reproducibility of the results. All datasets and analysis scripts are publicly available through Zenodo (Hajimirzaei, 2025).

2–3. Identification and Classification of Dusty Days

2–3–1. Data

Daily meteorological and aerosol data for Sanandaj (35.31°N, 47.00°E) were obtained from the CAMS EAC4 reanalysis produced by ECMWF, providing three hourly fields at 0.75° spatial resolution for the period 2003/01/01 to 2024/07/30. CAMS EAC4 was selected due to its long term temporal coverage and its consistent representation of aerosol and meteorological variables relevant to dust studies. From this dataset, aerosol optical depth at 550 nm (AOD550), dust aerosol optical depth (DUAOD550), and near-surface PM_{10} concentrations were extracted and aggregated to daily values.

To complement CAMS, daily dust optical depth (DOD) was obtained from the MERRA-2 reanalysis (variable mean_M2T1NXAER_5_12_4_DUEXTTAU). Previous studies have demonstrated the reliability of MERRA-2 for simulating mineral dust over the Middle East (Buchard et al., 2017; Randles et al., 2017). Based on their complementary physical meaning, four core indicators, PM_{10}, AOD550, DUAOD550, and DOD, were selected for the objective identification of dusty days. PM_{10} represents surface level particulate pollution and is directly linked to air quality and health impacts (WHO, 2021; USEPA, 2012). AOD550 captures the total column aerosol burden and is widely used as a proxy for dust activity in arid regions (Ginoux et al., 2012). DUAOD550 isolates the mineral dust contribution from total aerosols, allowing separation of natural dust from anthropogenic particles (Inness et al., 2019). DOD from MERRA-2 exclusively represents mineral dust, independent of other aerosol species, thereby enhancing detection robustness (Randles et al., 2017). These reanalysis products are grid- based datasets rather than point measurements. For this study, the grid cell containing Sanandaj (nearest grid point to 35.31°N, 47.00°E) was extracted. CAMS EAC4 provides fields at 0.75° (~80 km) spatial resolution, while MERRA-2 DOD data were used at 0.5° × 0.625°

(~50–60 km) resolution, ensuring adequate regional representation of dust conditions over western Iran.

Independent validation data were derived from surface METAR observations at Sanandaj Airport (OICS), retrieved from the Iowa Environmental Mesonet for the period 2003/01/01–2024/07/31. Dust related weather codes (DU, DS, SA, and HZ) were used to construct two daily binary validation datasets: a comprehensive definition including all four codes and a stricter definition limited to DU, DS, and SA. Daily dust occurrence was defined by the presence of at least one dust-related report per day, enabling an independent assessment of the dusty day classification derived from the reanalysis and indicators.

Figure 2 summarizes the overall methodological framework, illustrating the two main components of the study: (i) the derivation of quantitative thresholds and objective identification of dusty days using multi-source indicators, and (ii) the subsequent application of these identified dusty days for trajectory-based transport and source attribution analyses.

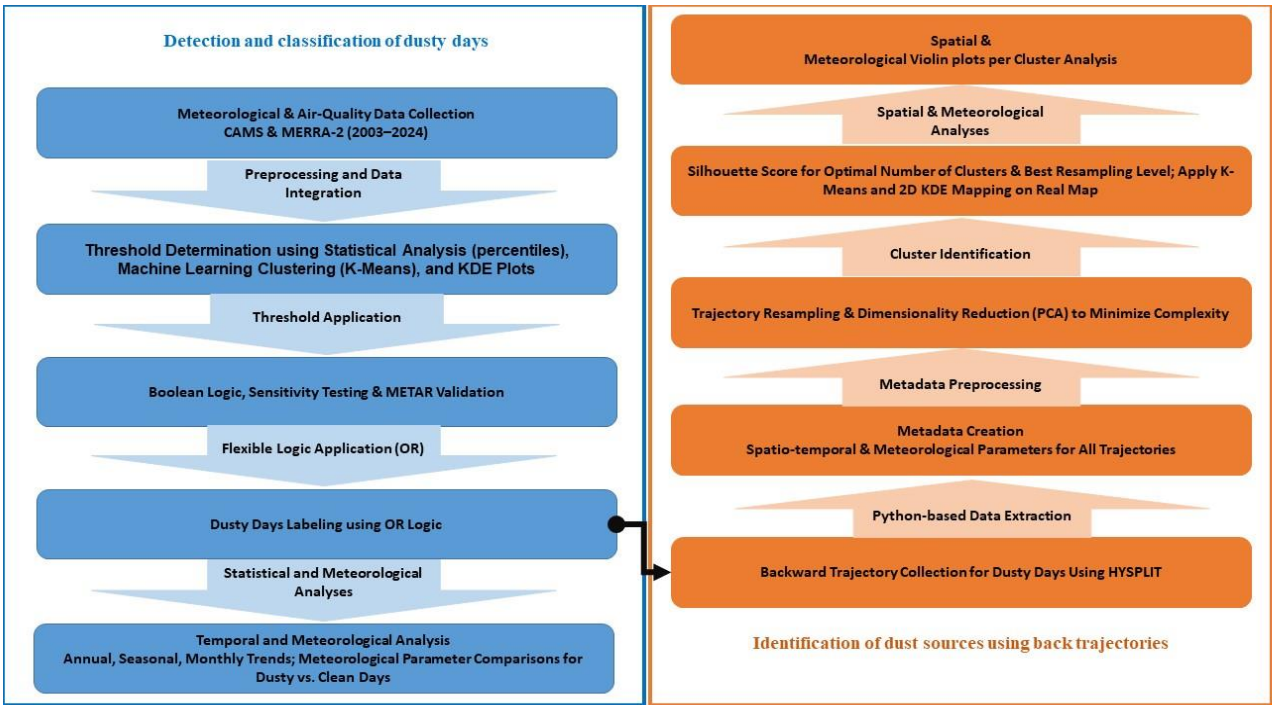

Figure 2. Workflow of the methodological framework for dusty-day detection and source attribution.

2–3–2. Data Normalization and Clustering-Based Identification of Dusty Days

Given the episodic and strongly skewed nature of dust variables, the identification of dusty days was guided by upper-tail statistical behavior rather than central tendency measures, as commonly reported for environmental datasets (Bakouch et al., 2020). A percentile-based analysis was therefore applied to distinguish anomalous dusty conditions from background variability and to characterize the intensity range of events, with particular emphasis on higher quantiles that represent rare and extreme dust episodes (Camuffo et al., 2018). In addition, correlation analysis among PM_{10}, AOD_{550}, $DUAOD_{550}$, and DOD was conducted to examine their interrelationships and complementarity, supporting their joint use within a unified dusty-day identification framework (Liao et al., 2006).

To objectively separate dusty from non-dusty conditions, an unsupervised K-Means clustering scheme was applied to the four indicators after Z-score normalization, ensuring equal contribution of each variable in Euclidean feature space (Jain, 2010). The number of clusters was fixed at k = 2, consistent with the binary classification objective of the study. This data-driven classification distinguishes statistically different regimes in the multivariate indicator space and provides the analytical basis for deriving quantitative thresholds and subsequently designing Boolean decision rules.

2–3–3. Kernel Density Estimation (KDE) for Data-Driven Threshold Extraction

To complement the clustering results and support objective threshold definition, Kernel Density Estimation (KDE) was employed as a non-parametric, distribution-based approach. KDE enables direct estimation of probability density functions without assuming a predefined distribution, which is appropriate for dust-related variables that commonly exhibit non-normal and heavy-tailed behavior (Scott, 2015; Pelz et al., 2023).

Following the K-Means classification (k = 2), KDE was applied separately to each cluster for PM_{10}, AOD_{550}, DOD, and $DUAOD_{550}$ in order to compare their distributional structures. The resulting density curves provided key reference features for threshold selection, including the intersection point between the clean and dusty clusters as a data-driven separation boundary, the dominant peak of the dusty cluster, relevant upper-tail percentiles for sensitivity assessment, and representative central tendency measures. Together, these features offered a coherent statistical basis for selecting robust and physically meaningful thresholds. By integrating KDE with the clustering outcomes, threshold determination was directly anchored to the empirical distributional behavior of the indicators rather than arbitrary fixed values, thereby strengthening transparency and methodological consistency before implementing the final Boolean decision logic.

2–3–4. Threshold determination and Boolean logic for dusty day identification

Final thresholds for PM_{10}, AOD550, DUAOD550, and DOD were derived through a data-driven procedure tailored to Sanandaj, integrating clustering, KDE, and percentile analyses. This avoided reliance on generic standards and ensured locally valid, robust cutoffs. A twostage Boolean logic framework was then established, distinguishing core parameters (DOD, DUAOD550) from general indicators (PM_{10}, AOD550). This separation improved classification accuracy and aligned with methodologies from international studies (Sorek-Hamer et al., 2013).

Eq. 1 $$\{[(X_{DOD} \geq T_{DOD}) \wedge (X_{DUAOD550} \geq T_{DUAOD550})] \wedge [(X_{Pm10} \geq T_{Pm10}) \vee (X_{AOD550} \geq T_{AOD550})]\}$$

Eq. 2 $$\{[(X_{DOD} \geq T_{DOD}) \vee (X_{DUAOD550} \geq T_{DUAOD550})] \wedge [(X_{Pm10} \geq T_{Pm10}) \vee (X_{AOD550} \geq T_{AOD550})]\}$$

The strict logic (AND), expressed in Equation (1), required both core parameters to exceed their thresholds and at least one general indicator to surpass its cutoff for a day to be classified as dusty. Conversely, the flexible logic (OR), defined in Equation (2), labeled a day as dusty if at least one core parameter and one general indicator exceeded their respective thresholds. This Boolean framework provided both conservative and sensitive modes of detection, ensuring a balanced, transparent, and reproducible system for dusty day identification.

2–3–5. Sensitivity analysis with respect to thresholds

To evaluate the robustness of the dusty day identification framework, a numerical sensitivity analysis was performed by perturbing the final thresholds of PM_{10}, AOD550, DUAOD550, and DOD. Each threshold was systematically varied by ±2% around its baseline value to account for measurement uncertainty and natural variability. This resulted in three levels per parameter (−2%, baseline, +2%) and a total of 81 threshold combinations. For all scenarios, the Boolean decision structure was held constant and the OR logic was applied. The number of identified dusty days was computed for each threshold combination, and sensitivity was assessed by examining the range and relative variation of detected events compared to the baseline configuration. This analysis quantified the extent to which small perturbations in threshold values influenced dusty day detection and provided an objective measure of the stability and reliability of the proposed framework.

2–3–6. Independent Validation Using METAR Ground Observations

To provide an independent out-of-sample validation of the proposed framework, ground METAR observations from Sanandaj Airport (OICS) were used as an external reference. METAR reports, combining human observations and automated measurements, are widely employed for documenting dusty weather phenomena and offer a reliable benchmark for validation. Two daily reference labels were defined: a comprehensive category (dusty_all), including DU, DS, SA, and HZ codes, and a stricter category (dusty_strict), limited to DU, DS, and SA. Model-based dusty day classifications obtained under both AND and OR Boolean logics were evaluated against these two reference definitions, resulting in four validation scenarios. Performance was assessed using confusion matrix metrics, including accuracy, precision, recall, and F1-score, with particular emphasis on recall to reflect the framework's ability to capture observed dust events. This validation step enabled an objective comparison of decision logics and provided independent evidence of the robustness and practical reliability of the proposed identification approach.

2-4. Identifying the source of dust storms

2–4–1. HYSPLIT model and backward trajectory data

To identify the potential source regions of dust events affecting Sanandaj, backward trajectories were computed using the NOAA HYSPLIT model, a widely applied tool for atmospheric transport and source attribution studies (Stein et al., 2015). 72 hour backward trajectories were generated for all 616 dusty days identified during the period 2003 to 2024, with Sanandaj (35.31°N, 46.98°E) specified as the arrival location. Trajectory simulations were performed using standard HYSPLIT configurations, and the resulting hourly trajectory coordinates were extracted and compiled into a unified dataset for subsequent statistical processing. This trajectory dataset formed the basis for dimensionality reduction, clustering, and classification of dominant dust transport pathways in later stages of the analysis.

2–4–2. Trajectory Preparation, Resampling, and Dimensionality Reduction

To prepare the HYSPLIT back trajectories for clustering and source attribution, all 72-hour trajectories were first organized in a consistent backward-time order to represent air-mass transport toward Sanandaj. To reduce data redundancy and ensure comparability among trajectories, uniform temporal resampling was applied, retaining representative points at fixed intervals along each trajectory. Multiple resampling resolutions were tested to balance structural preservation with computational efficiency.

The resampled trajectory coordinates were then arranged into a multivariate feature space for pattern analysis. Given the high dimensionality of this representation, Principal Component Analysis (PCA) was employed to reduce dimensionality while preserving the dominant variance structure of the trajectories (Jolliffe, 2002). The leading principal components, explaining the vast majority of total variance, were retained to project the trajectories into a low-dimensional space suitable for visualization and clustering.

This dimensionality reduction step removed redundant spatial correlations, enhanced interpretability, and enabled efficient identification of dominant transport patterns. The resulting reduced trajectory representation provided the analytical foundation for subsequent clustering and objective classification of dust source regions.

2–4–3. Determining the number of clusters using the silhouette score

Following dimensionality reduction of the back trajectories, the optimal number of clusters for K-Means was determined using the silhouette score, an internal validity index that quantifies cluster cohesion and separation (Rousseeuw, 1987). Because K-Means is an unsupervised method, the silhouette score was employed to objectively evaluate clustering performance without relying on external labels.

K-Means clustering was performed for a range of cluster numbers (K = 2 to 9), and average silhouette scores were computed for each configuration. This analysis was repeated for different trajectory resampling resolutions to assess the sensitivity of cluster structure to data density. Across all tested configurations, the highest and most stable silhouette scores were consistently obtained for K = 2, indicating the presence of two dominant and well-separated transport patterns. The robustness of this result across multiple resampling levels supports the interpretation that dust transport toward Sanandaj is governed by two primary trajectory regimes. These clusters form the basis for subsequent physical interpretation and source attribution of dust events.

2–4–4 Application of the final K-Means model and cluster characteristics

Following dimensionality reduction of the 72-hour backward trajectory dataset using Principal Component Analysis, K-Means clustering was applied with the number of clusters set to K = 2. The clustering was performed on the PCA reduced trajectory features to group air-mass pathways with similar transport characteristics. For spatial analysis, the arrival point coordinates of the clustered trajectories at the receptor location (Sanandaj) were extracted and analyzed using two dimensional Kernel Density Estimation. This approach was employed to examine the spatial distribution of trajectory endpoints for each cluster.

Temporal characteristics of the clusters were assessed by evaluating their seasonal and monthly occurrence. To characterize the atmospheric conditions associated with the transport pathways, meteorological variables including surface pressure, air temperature, relative humidity, precipitation, and mixed layer depth were analyzed along the 72-hour trajectories. In addition, integrated trajectory metrics, including total transport distance and mean transport velocity, were calculated to support comparative analysis between clusters.

3. Results and Discussion

3.1 Statistical Analysis and Relationships among Dust Parameters

The statistical behavior of PM_{10}, AOD550, DOD, and DUAOD550 was examined to support objective threshold selection and subsequent source interpretation. Mean values of 33.4 $\mu g/m^3$, 0.225, 0.099, and 0.072, respectively, contrast with systematically lower medians, indicating right-skewed distributions (Table 1). This skewness reflects the dominance of low background conditions punctuated by infrequent but intense dust episodes, a well-known characteristic of dust prone environments, and provides a strong rationale for using data-driven, non-linear approaches rather than fixed or normal approach assumptions (Bartoletti & Loperfido, 2009).

Table 1. Descriptive statistics of the dust-related parameters (PM_{10}, AOD550, DOD, and DUAOD550) during the study period (2003–2024)

Parameters	PM_{10} $\mu g\ m^{-3}$	AOD550	DOD	DUAOD550
Count	7882	7882	7882	7882
Mean	33.4	0.225	0.099	0.072
STD	27.21	0.16	0.087	0.081
Min	0	0.0028	0.002	0
50%	26.545	0.189	0.077	0.048
Max	293.60	1.44	0.745	0.785

To characterize the upper tail, percentiles between the 75th and 99th were evaluated (Table 2). All parameters show sharp escalation beyond the 90th percentile, particularly between the 90th, 95th, and 99th levels. For example, PM_{10} increases from 64.32 $\mu g/m^3$ at P90 to 140.3 $\mu g/m^3$ at P99, while similar jumps occur in AOD550, DOD, and DUAOD550. These steep gradients confirm that dust loading is controlled by a relatively small number of severe events, supporting the use of upper percentiles as meaningful statistical benchmarks for defining dusty conditions (Adamkiewicz et al., 2021).

Table 2. Upper percentile values (75th to 99th) of dust-related parameters (PM_{10}, AOD550, DOD, and DUAOD550)

Parameters	75%	80%	85%	90%	95%	99%
PM_{10} $\mu g\ m^{-3}$	41.65	46.58	53.62	64.32	85.3	140.3
AOD550	0.29	0.32	0.36	0.43	0.54	0.82
DOD	0.13	0.15	0.17	0.21	0.27	0.42
DUAOD550	0.095	0.11	0.13	0.16	0.23	0.38

Frequency distributions and KDE curves (Figure 3) further confirm strong positive skewness. DOD and DUAOD550 are highly clustered near zero with long right tails, whereas PM_{10} and AOD550 exhibit broader spreads but maintain similar asymmetry. As medians are more representative of central tendency than means, traditional central indices are inadequate for discriminating dusty from non-dusty conditions. Instead, emphasis on upper percentiles (particularly 90th to 95th) is more appropriate for capturing episodic dust behavior within the methodological framework (Ginoux et al., 2012).

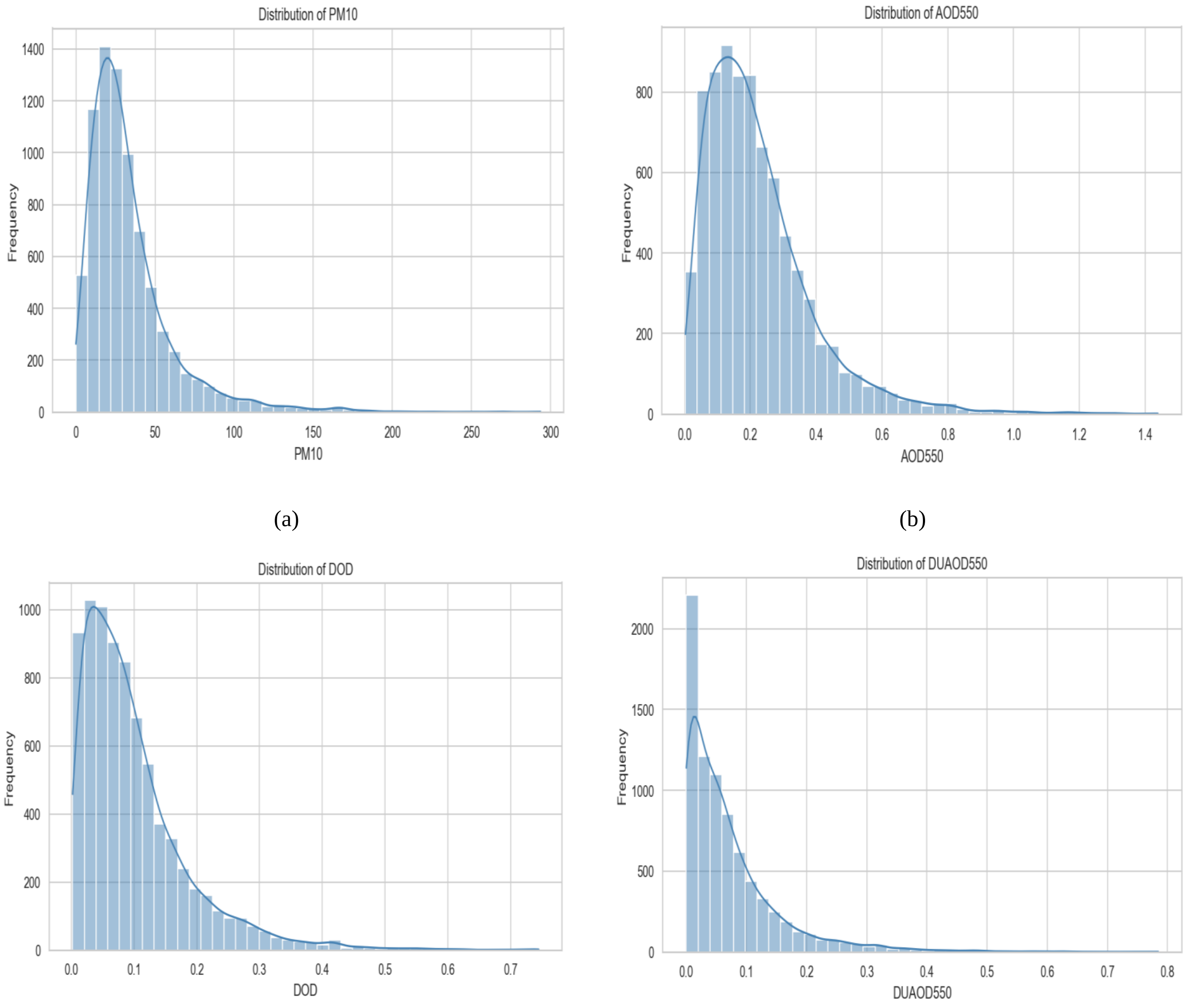

(a) (b) (c) (d)

Figure 3. Frequency distributions and Kernel Density Estimates (KDE) plots for parameters: (a) PM_{10}, (b) AOD550, (c) DOD, and (d) DUAOD550

The Pearson correlation matrix (Figure 4) reveals strong and coherent relationships among CAMS and MERRA-2 indicators. DUAOD550 shows the highest correlation with surface PM_{10} (r = 0.89), confirming its reliability as a near-surface dust proxy. AOD550 also correlates well with PM_{10} (r = 0.84) and DUAOD550 (r = 0.87), indicating that total column aerosol loading in this region is largely dust-dominated. Likewise, MERRA-2 DOD exhibits strong agreement with CAMS variables (r = 0.78–0.84), reinforcing its value as a dust-specific metric. Collectively, these strong correlations demonstrate that aerosol optical properties in the study domain are primarily dust-driven, strengthening confidence in the multi-source framework and providing a solid statistical basis for subsequent thresholding and event identification.

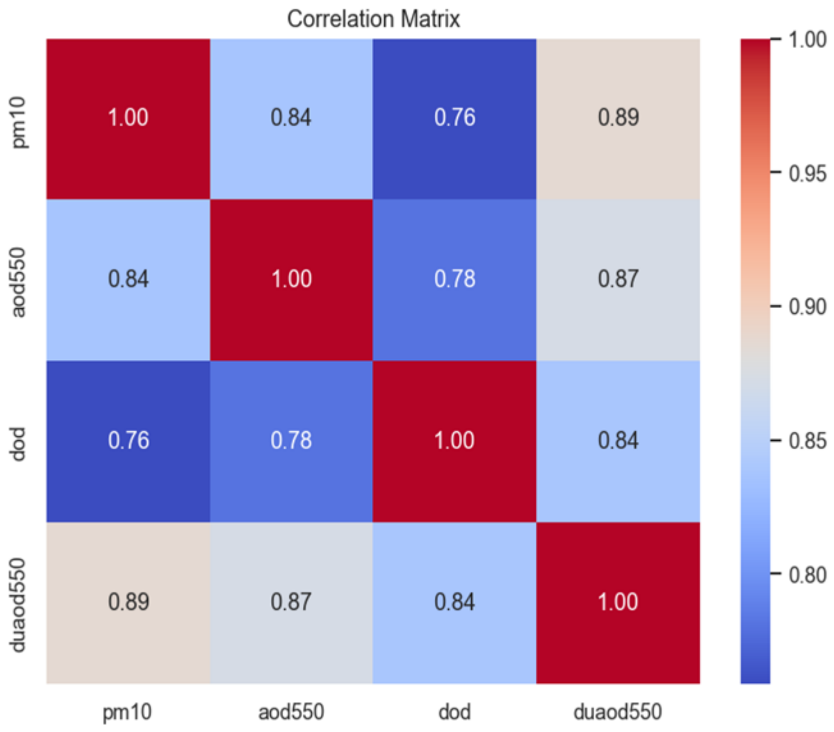

Figure 4. Pearson correlation matrix among key dust-related parameters: PM_{10}, AOD550, DOD, and DUAOD550

3.2. Data-Driven Thresholds and Dust Day Labeling

Initial analyses revealed that PM_{10}, AOD550, DOD, and DUAOD550 exhibit positively skewed, non-Gaussian distributions with strong interdependencies, indicating the coexistence of frequent background conditions and fewer, yet intense, dust outbreaks. To objectively distinguish these contrasting regimes, K-Means clustering was first applied after Z-score normalization. The algorithm naturally converged to two statistically distinct groups, corresponding to normal and dusty conditions. As summarized in Table 3, Cluster 0 is characterized by substantially lower mean values, whereas Cluster 1 displays markedly elevated PM_{10}, AOD550, DOD, and DUAOD550, with differences exceeding a factor of 2–5 depending on the parameter.

Clusters	PM_{10} (μg/m³)	AOD550	DOD	DUAOD550

Clean 0	23.88	0.167	0.069	0.042
Dusty 1	74.91	0.476	0.231	0.202

Table 3. Mean values of dust-related parameters for the two K-Means clusters: Cluster 0 (Clean) and Cluster 1 (Dusty)

These contrasts indicate a clear physical separation between clean-air and dust-dominated states. Moreover, the mean values of Cluster 1 closely align with the 90th–95th percentiles of the full dataset, confirming that this cluster represents genuinely severe dust episodes rather than moderate fluctuations. The pairwise scatter distributions shown in Figure 5 further highlight this behavior, with Cluster 1 systematically occupying the upper-value domain and confirming the bimodal and objectively separable nature of the systems.

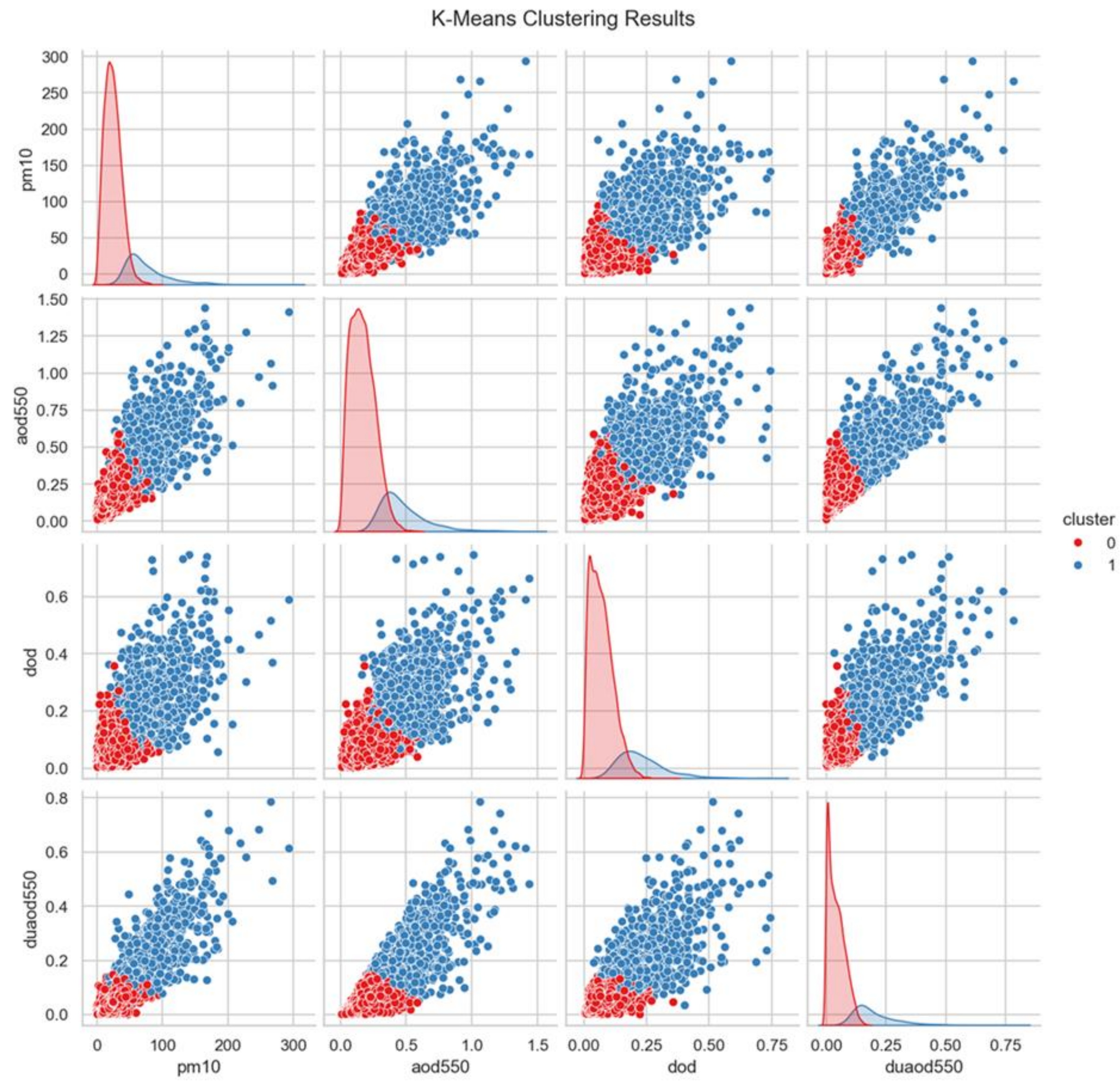

Figure 5. Pairwise scatter plots (Pair plot) of dust-related parameters (PM_{10}, AOD550, DOD, and DUAOD550) based on K-Means clustering

While clustering establishes a clear regime distinction, defining meaningful operational thresholds requires quantifying where dusty conditions become more probable than normal background variability. To address this, Kernel Density Estimation (KDE) was applied to the cluster-separated distributions of each parameter.

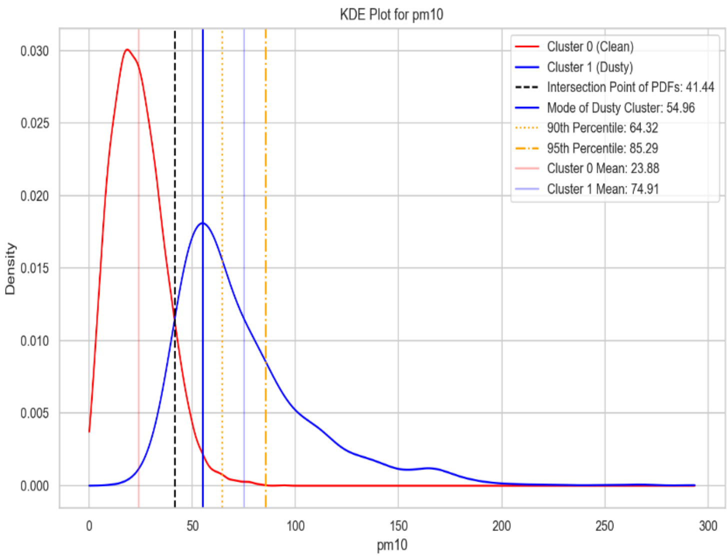

(a)

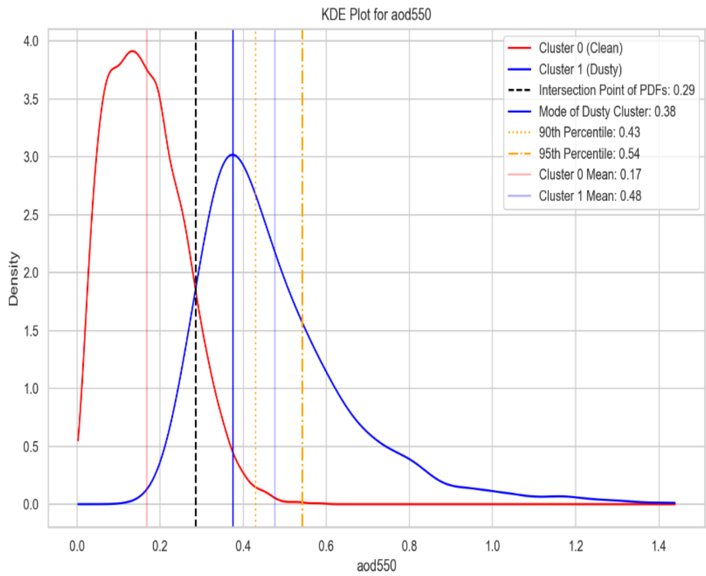

(b)

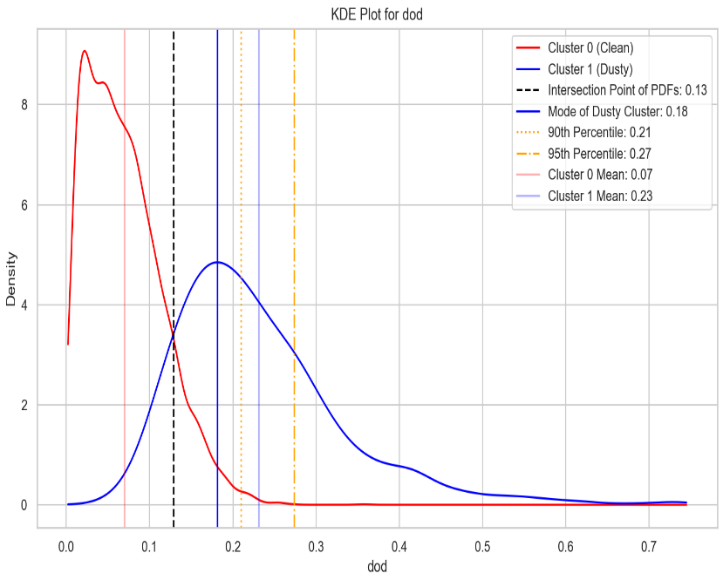

(c)

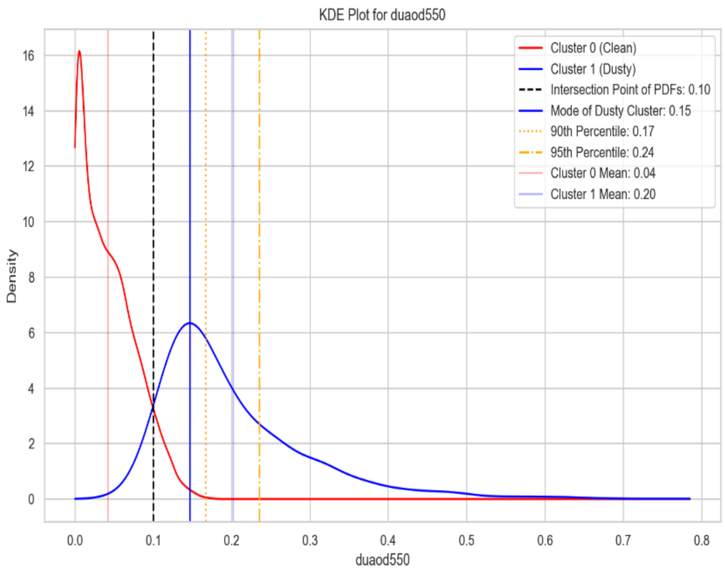

(d)

Figure 6. Kernel Density Estimate (KDE) Plots by K-Means Clusters (2 Clusters) for parameters: (a) PM_{10}, (b) AOD550, (c) DOD, and (d) DUAOD550

The KDE curves in Figure 6 illustrate the probability structure of normal and dusty conditions, highlighting the intersection point as the level where the dominance shifts from background to dust-driven behavior. This transition point, together with the dusty-mode values and the upper percentiles, provides an integrated representation of core event intensity, rarity, and regime separation. These key statistical markers, summarized in Table 4, ensure that threshold selection is grounded simultaneously in probability structure, clustering behavior, and empirical distribution characteristics rather than arbitrary assumptions (Lin et al., 2011; Ruckthongsook et al., 2018).

Table 4. Statistical Summary of Key Distribution Metrics for Each Parameter Used in Dusty Day Threshold Determination

Parameter	Intersection Point of PDFs	Mode of Dusty Cluster	90th Percentile	95th Percentile	Cluster 0 Mean	Cluster 1 Mean
PM_{10} (µg/m³)	41.44	54.96	64.32	85.29	23.88	74.91
AOD550	0.286	0.375	0.429	0.542	0.17	0.476
DOD	0.128	0.1812	0.2097	0.27	0.069	0.23
DUAOD550	0.0998	0.1461	0.17	0.235	0.04	0.202

Based on this combined evidence, $PM_{10} \geq 75$ µg/m³ was adopted as the data-driven cutoff, as it exceeds the KDE crossover and dusty mode, closely matches the dusty cluster mean, and lies within the 90th-95th percentile range, thereby capturing genuinely high concentration events. Similarly, AOD550 ≥ 0.45 was selected because it is higher than both the intersection and mode, aligns with the dusty cluster mean, and falls within the upper percentile domain, ensuring sensitivity to substantial aerosol loading. For DOD, a threshold of ≥ 0.20 was defined, clearly above the crossover and near the 90th percentile, which is consistent with physically meaningful enhancement of coarse dust contributions. The same value was assigned to DUAOD550, exceeding the KDE intersection and dusty mode, consistent with the dusty cluster mean and approaching the 95th percentile, enabling reliable detection of intense pure dust conditions while avoiding contamination from weaker or mixed aerosol states.

Overall, combining K-Means clustering with KDE analysis provided a coherent and physically meaningful framework for distinguishing dusty from non-dusty regimes. The resulting thresholds emerge directly from the statistical behavior of the data, are internally consistent across multiple independent indicators, and are therefore objective, reproducible, and operationally robust. These rigorously defined cutoff values constitute the basis for subsequent dusty day identification and analysis in this study.

3-2-1. Evaluation of Logical Approaches and Sensitivity Analysis

Once the data-driven thresholds were established, they were applied to the full study period to identify dusty days and to assess the robustness of the decision framework. Two logical strategies were evaluated: a strict "AND" configuration, requiring simultaneous exceedance of all thresholds, and a more flexible "OR" rule, triggered when any single indicator exceeds its cutoff. Using the adopted limits (PM_{10} ≥ 75 μg/m³, AOD550 ≥ 0.45, DOD ≥ 0.20, DUAOD550 ≥ 0.20), the AND logic identified 406 dusty days, whereas the OR logic detected 616 events, adding 210 cases and representing nearly a 50% increase. All AND detected days were captured by OR, showing that AND mainly represents intense, high confidence events, while OR additionally detects marginal or localized dust conditions and instances of limited synchronization between surface and satellite signals (Stieb et al., 2008; Kaskaoutis et al., 2008). Thus, the two strategies characterize different segments of the dust continuum rather than producing conflicting outcomes.

Threshold stability was further examined through sensitivity testing by perturbing each cutoff by ±2%, generating 81 combinations. This adjustment reflects realistic observational and retrieval uncertainties (Pisoni et al., 2018). Under the OR rule, detected dusty days ranged from 580 to 644 (≈10.4% variation), while AND varied between 382 and 422 (≈9.9% variation). These modest fluctuations demonstrate that both approaches remain stable under perturbation, confirming that the framework is not overly sensitive to small threshold deviations. Nevertheless, their functional distinction persists: OR consistently offers broader sensitivity suited to climatological monitoring, whereas AND remains conservative and better aligned with applications requiring high event certainty.

Independent validation using METAR observations from Sanandaj Airport (2003-2024) provided an external performance assessment. Two validation references were constructed: a broader reconstruction including DU, DS, SA, and HZ (301 days) and a stricter one excluding haze (224 days). Both logics yielded high accuracy (OR: 0.906-0.915; AND: 0.927-0.936), reflecting the dominance of non-dusty days. However, their precision, recall behaviour diverged. OR achieved higher recall (0.309-0.393), indicating stronger capability to capture recorded dust events, though with lower precision (0.151-0.143). Conversely, AND produced higher precision (0.165-0.158) but lower recall (0.223-0.286), meaning more conservative detection with some underestimation. These outcomes align with the conceptual design of both schemes and confirm their complementary strengths: OR minimizes missed events, while AND reduces false alarms.

3-3. Temporal, Climatic and Synoptic Features of Dusty Days

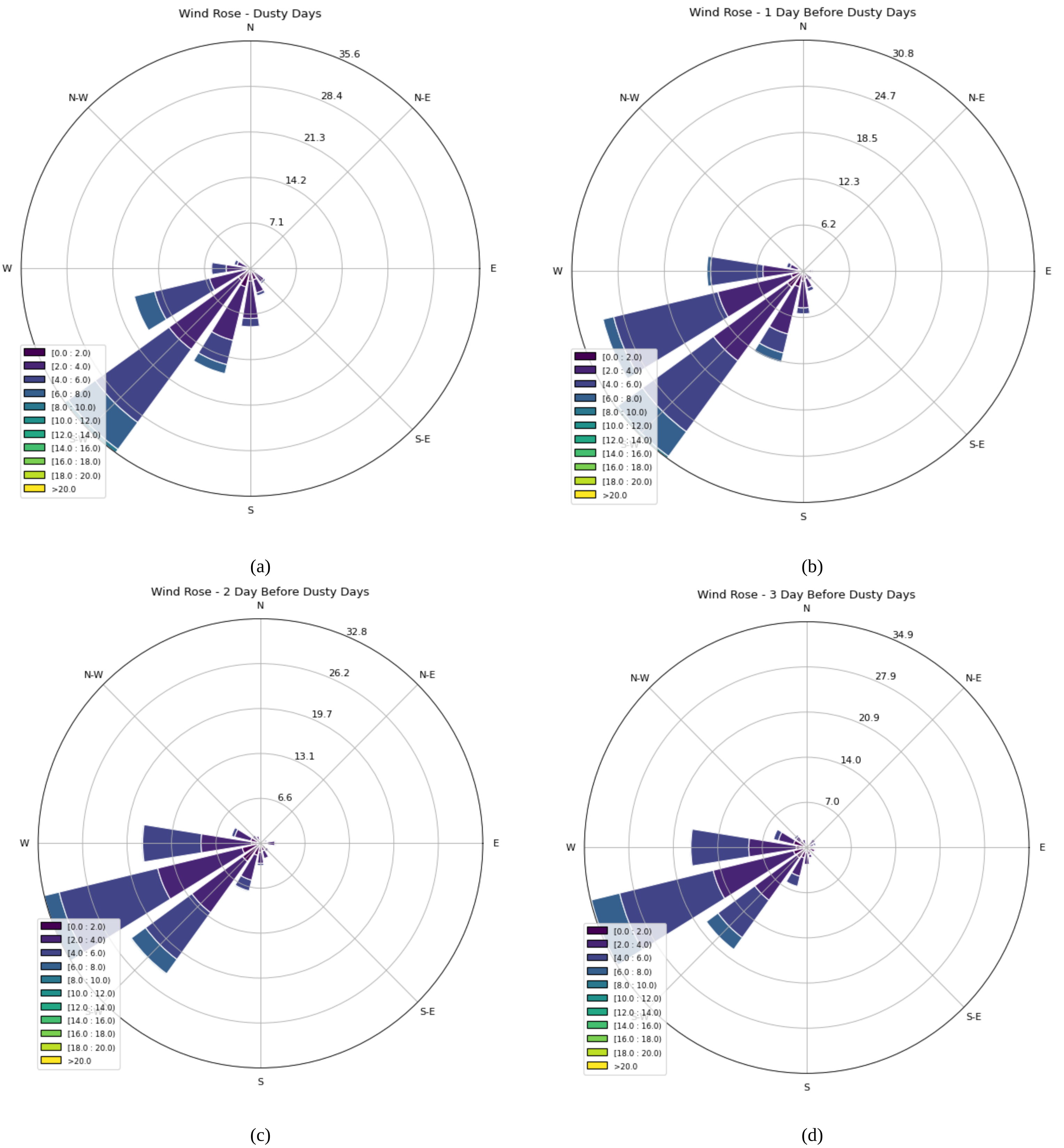

(a) (b) (c) (d)

Figure 7. Wind Rose for (a) Dusty Days, (b) One Day Before Dusty Days, (c) Two Days Before Dusty Day, and (d) Three Days Before Dusty Days

Overall, the integration of logical comparison, sensitivity testing, and independent validation demonstrates that the framework is statistically stable, operationally reliable, and scientifically interpretable. OR is better suited for comprehensive long-term monitoring, whereas AND represents a stricter subset of intense, high-confidence events, together offering a flexible and robust basis for dust climatology and risk assessment.

3-3-1. Wind Rose and Dominant Patterns

Wind rose analysis for the 616 identified dust days and the preceding three days (Figs. 7a-d) shows a clear dominance of southwesterly (35%) and southwesterly-westerly (18%) flows, with typical speeds of 2-6 m s^{-1} and occasional intensification beyond 8 m s^{-1}. These patterns indicate cross border transport primarily from the Mesopotamian Plains and Syrian Desert. One to three days before events, wind speeds are weaker (<5 m s^{-1}) and directions more dispersed, while southwesterly dominance strengthens progressively toward the event day. This transition from diffuse to intensified directional flow reflects approaching synoptic disturbances that enhance pressure gradients and exceed the threshold required for dust emission and advection. Overall, the decisive control of SW and SW-W winds on dust activity is evident and agrees with regional findings (Bagherabadi & Moeinaddini, 2023; Hamzeh et al., 2021).

3-3-2. Temporal Patterns of Dust Day Occurrence

Annual variability (Fig. 8a) reveals pronounced peaks in 2009 (58 days), 2011 (47), and 2008 (42), contrasted with lower frequencies in 2005 and several recent years. This fluctuation is consistent with large-scale climate variability, regional drought, and circulation anomalies (Abadi et al., 2025). Seasonally (Fig. 8b), dust occurrence is strongly concentrated in spring (66.4%), followed by summer (21.6%), while autumn (5.0%) and winter (7.0%) contribute marginally. Monthly statistics (Fig. 8c) confirm maximum activity in May (170 days), April (156), and March (87). This timing coincides with enhanced synoptic activity, stronger southwesterlies, deeper boundary layers, and reduced soil moisture, all favorable for dust mobilization, whereas winter and late-autumn stability suppress outbreaks. These temporal characteristics are consistent with broader Iranian and Middle Eastern climatology (Sari Sarraf et al., 2016; Baghbanan et al., 2020). This seasonal enhancement is fully consistent with the well documented spring synoptic circulation over the Middle East, where frequent low pressure systems over Iraq and the Syrian Desert, together with prevailing southwesterly to westerly flows, intensify dust uplift and support long range transport toward western Iran (Mohammadpour et al., 2021).

3-3-3. Analysis of Meteorological Variables Related to Dust Days

Temperature distributions (Fig. 9a) indicate that dusty days predominantly occur between 10-30 °C, with a clear concentration around 15-20 °C. Such moderately warm conditions correspond to drier soils, enhanced turbulence, and deeper mixing layers that facilitate dust entrainment (UNEP, 2016; Middleton et al., 2019).

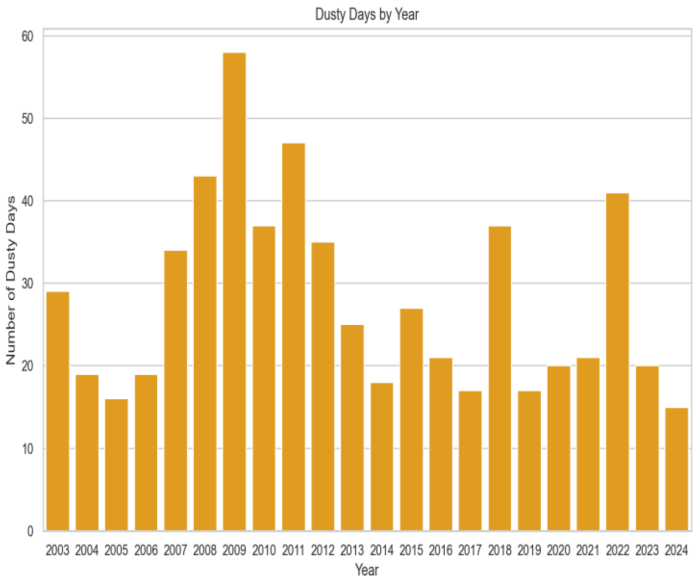

(a)

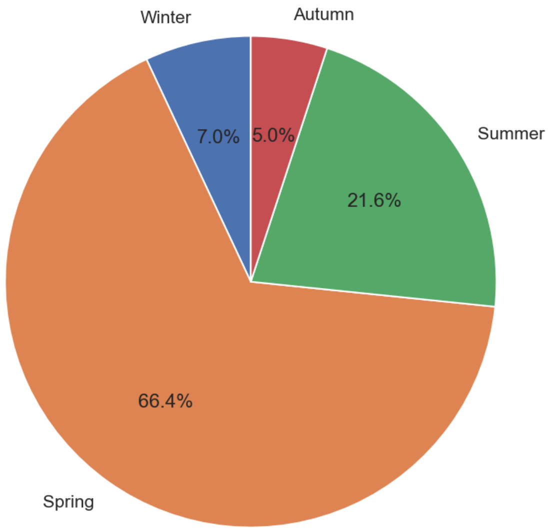

(b)

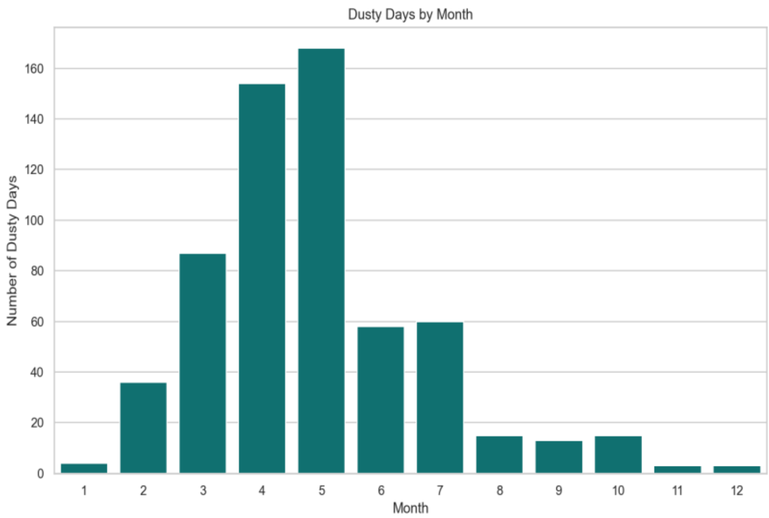

(c)

Figure 8. Temporal Distribution of Dusty Days in the Study Area: (a) Annual distribution (2003–2024), (b) Seasonal share, and (c) Monthly variation.

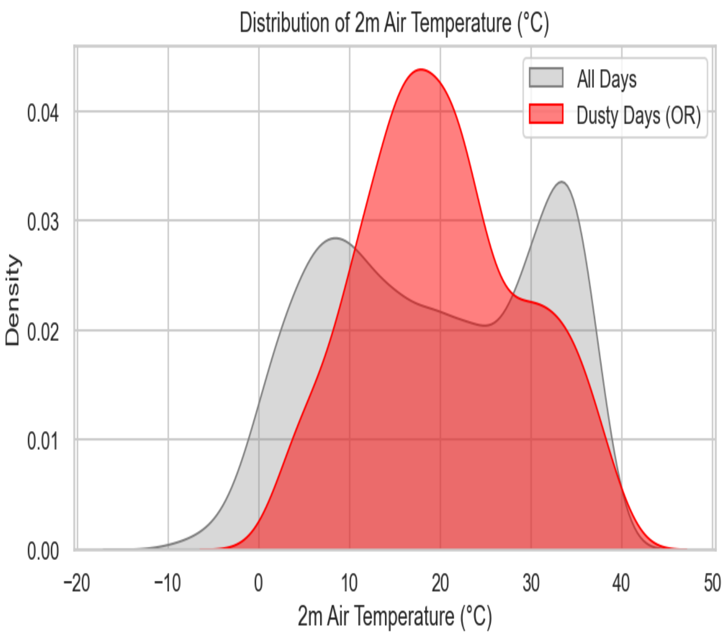

(a)

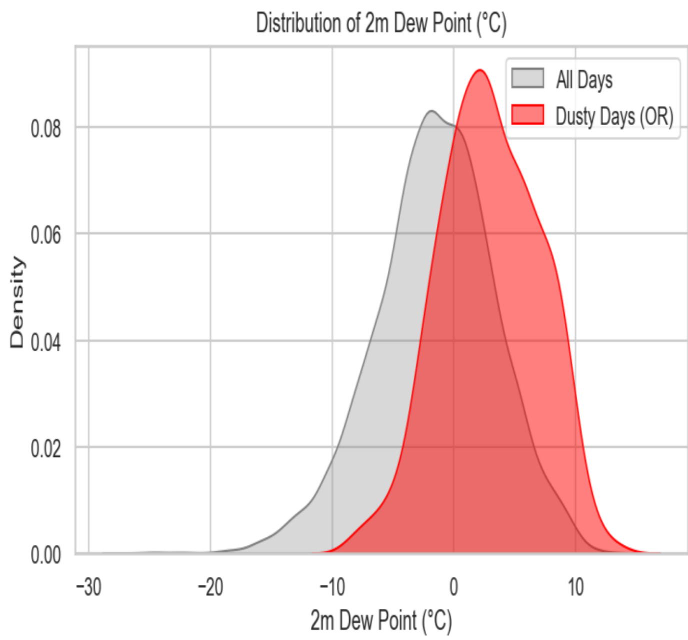

(b)

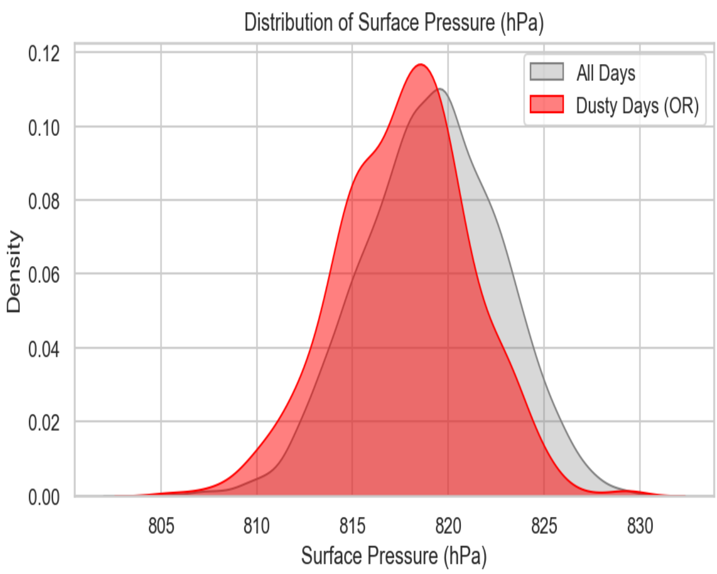

(c)

Figure 9. Density Distributions of Meteorological Parameters for Dusty and Non-Dusty Days: (a) Air Temperature, (b) 2-meter Dew Point Temperature, and (c) Surface Pressure.

Dew point distributions (Fig. 9b) cluster around 0-5 °C, slightly higher than climatology, implying modest absolute humidity but still relatively dry boundary layer conditions, consistent with springtime synoptic patterns across the Middle East (Rashki et al., 2021; Miri et al., 2021). Surface pressure (Fig. 9c) shows left-skewed distributions with peaks around 815-820 hPa, indicating the predominance of low-pressure systems that intensify horizontal gradients, strengthen southwesterly flow, and promote long-range transport. These meteorological signatures reinforce the wind-rose results and agree with previous synoptic analyses in the region (Barati et al., 2020; Bagherabadi & Moeinaddini, 2023; Hamzeh et al., 2021).

3-4. Analysis of Backward Trajectories

3-4-1. Definition of Backward Trajectories and Data Preparation

For each of the 616 dust days, 72-h back trajectories were simulated with HYSPLIT, initialized at 12:00 UTC and receptor fixed at Sanandaj. Starting altitudes were automatically set based on boundary layer height. Outputs provided sequential latitude-longitude positions of air parcels, along with variable trajectory lengths despite the fixed 72-h window. To standardize inputs for clustering, all trajectories were resampled to equal point counts (24, 12, and 6) to test robustness and sensitivity. Each trajectory was then flattened into a vector of sequential latitude-longitude pairs, creating high dimensional feature spaces (e.g., 48 features for 24 points).

3-4-2. Dimensionality Reduction and Clustering

To manage data complexity and improve clustering, PCA was applied, reducing high-dimensional trajectories to two principal components capturing most variance. The reduced data were then clustered with K-Means, an unsupervised algorithm that groups samples by intrinsic similarity without prior labels. The optimal number of clusters (K) was determined using the Silhouette Score, which measures intra-cluster cohesion and inter-cluster separation. Scores were computed for K = 2-9, with higher values indicating better structure. Results are shown in Table 5.

Table 5. Comparison of Silhouette Scores Across Varying Numbers of Resampled Trajectory Points and Clusters (K)

Number of clusters (K)	Silhouette Score for 24pts	Silhouette Score for 12pts	Silhouette Score for 6pts
2	0.4282	0.4296	0.4277
3	0.3593	0.3582	0.36
4	0.3838	0.3826	0.3838
5	0.3675	0.3636	0.3656
6	0.3499	0.3513	0.3813
7	0.3773	0.3747	0.3498
8	0.346	0.346	0.3486
9	0.3452	0.3621	0.3414

As shown in Table 5, the optimal number of clusters (Best K) was consistently 2 across all resampling scenarios (24, 12, and 6 points). This stability indicates the presence of two dominant and distinct transport patterns, corresponding to major dust sources affecting Sanandaj. For K = 2, silhouette scores of ~0.42–0.43 confirm meaningful and reliable separation between clusters. To balance detail preservation and computational efficiency, subsequent analyses adopt the two-cluster solution based on 12-point resampling. These clusters, labeled Cluster 0 and Cluster 1, are examined in the following sections to interpret their spatial and meteorological characteristics.

3-4-3. Spatial, Statistical, and Geographical Analysis of Backward Trajectory Clusters: Identifying Source Regions

Undrestanding the spatial behaviour of dust carrying air masses is essential for interpreting the

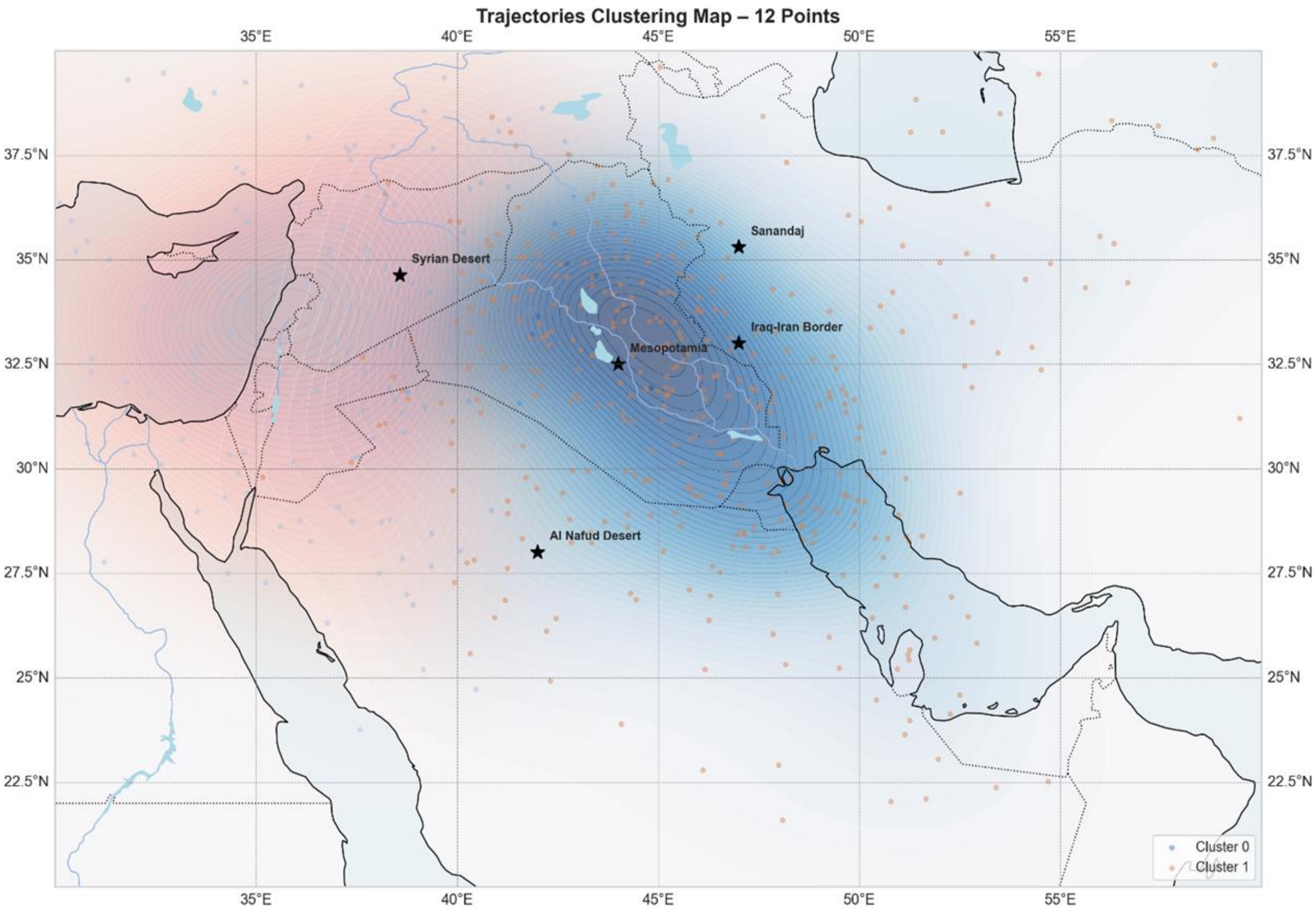

Figure 10. Clustered HYSPLIT back-trajectories (12 resampled points per trajectory), overlaid with the study area (Sanandaj) and known regional dust source regions

physical origin of dusty days in Sanandaj. After grouping the 72-h HYSPLIT backward trajectories into two clusters, their geographic patterns and transport characteristics were examined to identify dominant source regions. Figure 10 illustrates the clustered trajectories along with the location of Sanandaj and major recognized Middle Eastern dust reservoirs, including the Syrian Desert, Mesopotamian plains, the Iran-Iraq border region, Khuzestan, and the northern An-Nafud Desert (Givehchi et al., 2013; Moridnejad et al., 2015; World Bank, 2019; Lian et al., 2022).

Two clearly distinct advection regimes emerge. The first group (Cluster 0) consists of longer, west-northwesterly pathways originating mainly over the Syrian Desert and extending across northern and western Mesopotamia toward western Iran. These trajectories represent long range transport driven largely by westerly circulation, consistent with the synoptic systems reported for the region (UNEP, 2016; Salmabadi et al., 2023). The second group (Cluster 1) forms a denser and more frequent pattern, dominated by southern and south-westerly inflow from the southern Mesopotamian basin, the Iran-Iraq borderlands, Khuzestan, and, in some cases, the northern Arabian Peninsula. The high prevalence of this cluster indicates that regional to near regional transport plays the primary role in dust intrusions over Sanandaj.

Of the 616 dusty days, Cluster 1 accounts for 415 trajectories (67%), whereas Cluster 0 represents 201 cases (33%), demonstrating the predominance of southern and south-westerly sources. Spatial analysis further shows that Cluster 0 generally occupies more distant locations to the west and northwest of the study area, whereas Cluster 1 remains geographically closer and more confined to the Iraq-Iran corridor and adjacent Mesopotamian lowlands. To further substantiate these interpretations, the great circle distances between the centroid of each cluster and the major dust source regions were calculated (Table 6). These values quantitatively confirm that Cluster 0 is most closely associated with the Syrian Desert and western Mesopotamia, while Cluster 1 is strongly linked to nearby sources such as the Iran-Iraq border and southern mesopotamia.

Of the 616 dust days, Cluster 1 dominates with 415 trajectories (67%), compared to Cluster 0 with 201 (33%). This predominance shows that most dust events in Sanandaj are driven by southern transport pathways, underscoring the importance of southern Mesopotamia and southwestern Iran in mitigation strategies. Cluster 0, with a mean origin of 33.78°N, 33.98°E, corresponds mainly to the Syrian Desert and north/west Mesopotamia, reflecting more westerly pathways (Moridnejad et al., 2015; UNEP, 2016; Kutiel, 2003). Cluster 1, centered at 32.35°N, 47.07°E, points to southern Mesopotamia, the Iran-Iraq border, and northern Khuzestan, representing easterly and southerly sources. These results align with regional studies identifying the same areas as the principal dust sources for western Iran (Sotoudeheian et al., 2016; Beyranvand et al., 2023).

Overall, the trajectory analysis demonstrates a dual source framework for Sanandaj: a near regional, high frequency pathway from southern Mesopotamia and neighbouring border regions, and a secondary but climatologically important long range pathway from the Syrian Desert and western Middle East. This clear separation strengthens the physical interpretation of the clustering results and provides a robust basis for subsequent synoptic and seasonal source attribution. The distinction between these two regimes is physically meaningful, reflecting the coexistence of near source dust outbreaks governed by boundary layer processes and long range elevated transport controlled by synoptic-scale systems, a mechanism frequently reported for the Middle East (Mohammadpour et al., 2021).

Table 6. Distance (in km) from Known Dust Sources and the Study Area to the Center of Each Cluster

Cluster	Dust Source	Distance(km)	Cluster	Dust Source	Distance(km)
0	Syrian Desert	433.6	1	Iraq-Iran Border	72
0	Mesopotamia	945.4	1	Mesopotamia	288.8
0	An Nafud Desert	998.7	1	Sanandaj	326.9
0	Sanandaj	1206.4	1	An Nafud Desert	686
0	Iraq-Iran Border	1213.9	1	Syrian Desert	828.6

3-4-4. Analysis of Trajectory-averaged Meteorology Features per Clusters

Violin plots and mean values (Table 7) show clear meteorological contrasts between clusters. Pressure is systematically lower in Cluster 0 (815.02 hPa) than in Cluster 1 (859.19 hPa), indicating higher altitude transport (Mashat et al., 2020). In Fig. 11a, Cluster 0 displays a narrow, symmetric violin, reflecting a homogeneous pressure regime. In contrast, Cluster 1 shows broader variability with mild skewness, consistent with more heterogeneous regional-scale flows (Karami et al., 2021).

Table 7. Average Values of Key Meteorological Parameters, Pressure, Rainfall, Relative Humidity, and Potential Temperature, for Each Identified Cluster

Cluster	Pressure (hPa)	Rainfall (mm)	Relative Humidity (%)	Potential Temperature (C)
0	815.02	0.01	32.97	33.34
1	859.19	0.02	32.63	32.42

Rainfall is negligible for both clusters (medians: 0.01 vs. 0.02 mm). However, Cluster 1 shows an elongated upper tail (Fig. 11b), indicating occasional encounters with weak precipitation systems and modest wet removal (Niu et al., 2023).

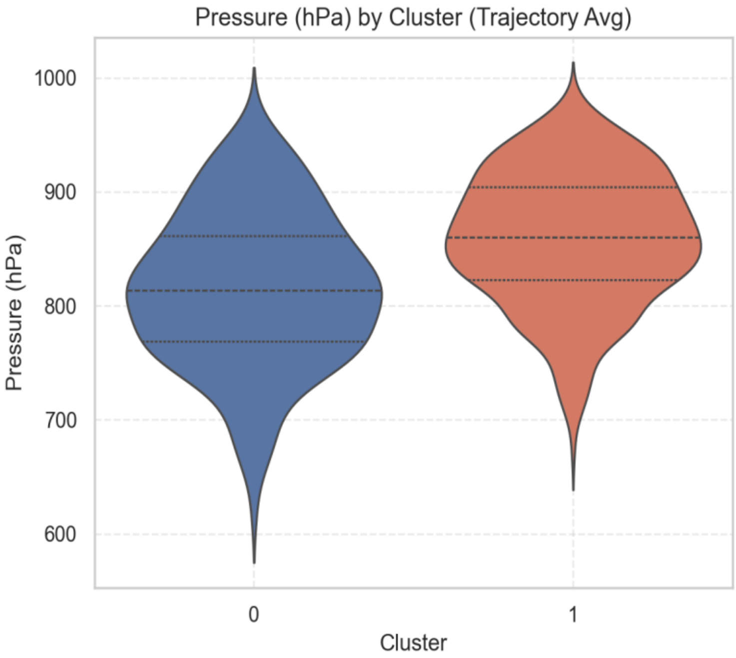

(a)

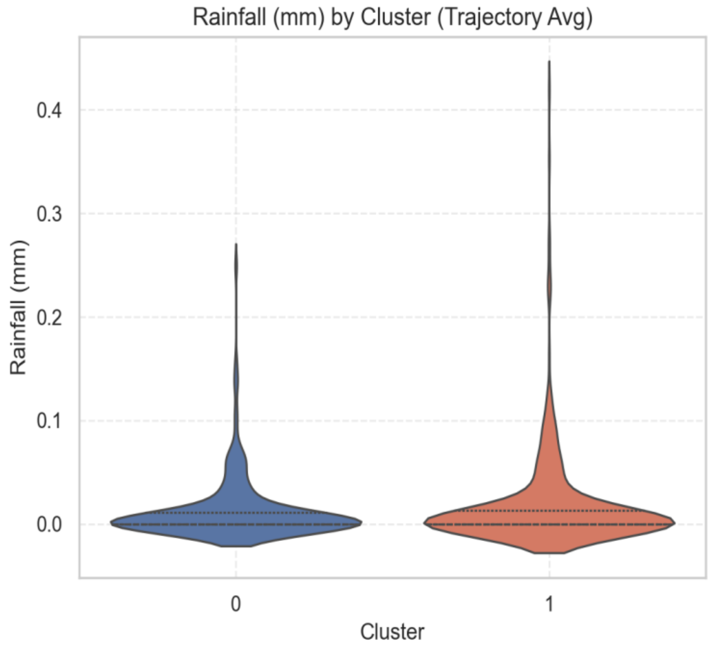

(b)

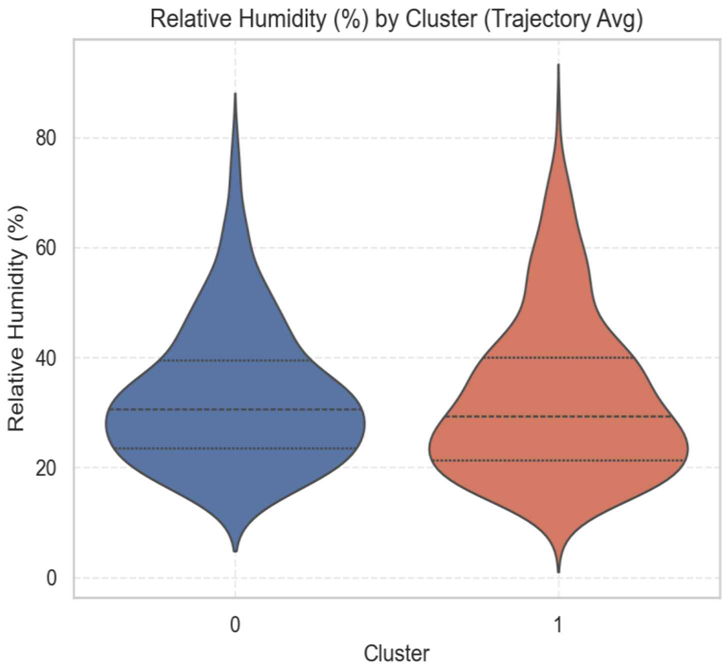

(c)

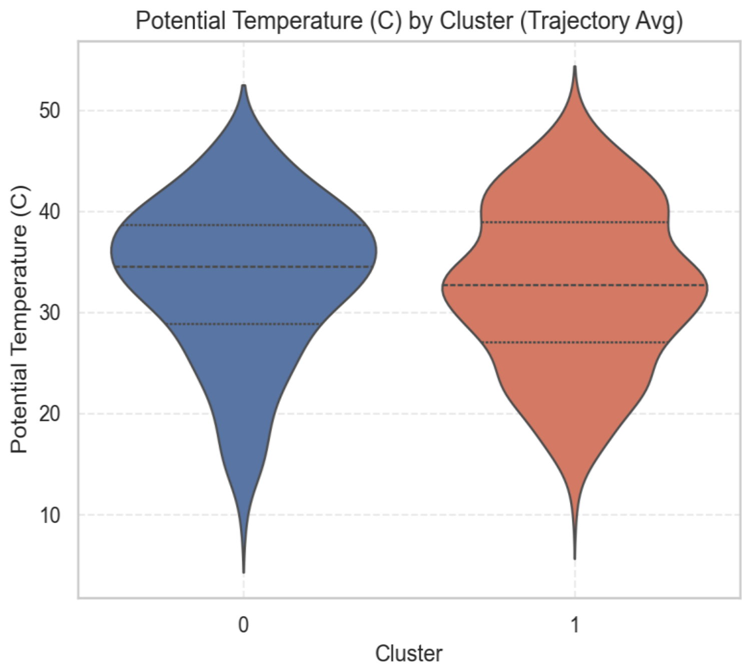

(d)

Figure 11. Violin plots of meteorological parameters (a) pressure (b) rainfall (c) relative humidity and (d) potential temperature per cluster.

The absence of such a tail in Cluster 0 highlights its dominance by dry, long range transport with minimal scavenging. Relative humidity (RH) has nearly identical means (~33%), but distributions differ (Fig. 11c). Cluster 1 displays a wider IQR and a secondary bulge, suggesting multimodal regimes shaped by boundary layer interactions and surface variability. Cluster 0, in contrast, is compact and skewed toward lower RH, confirming drier elevated transport (Ma et al., 2023).

The strongest contrast appears in potential temperature (θ), a thermodynamic indicator of stability (Fig. 11d). Cluster 0 shows systematically higher θ (33.34 °C) than Cluster 1 (32.42 °C), with a broad unimodal distribution centered at warmer, stable layers that favor long range advection and dust preservation. Cluster 1 has lower, narrower θ with occasional downward skewness, reflecting episodic mixing with cooler near surface air. This thermodynamic contrast substantiates the physical dichotomy, Cluster 0 represents long-range, elevated, stable transport, associated with dry conditions and efficient dust preservation, and Cluster 1 reflects regional, boundary layer influenced pathways, shaped by surface variability, weak precipitation, and moderate humidity (Fix et al., 2024).

3-5. General Discussion and Comprehensive Interpretation

This study proposed a data-driven framework for identifying dusty days and interpreting their transport behaviour in regions with limited ground observations. Integrating statistically derived thresholds with backward trajectory clustering provided a physically consistent characterization of dust occurrence and source attribution for Sanandaj, offering insights highly relevant for early warning and management strategies in western iran.

Statistical analyses of PM_{10}, AOD_{550}, $DUAOD_{550}$, and DOD revealed strongly skewed, non-normal distributions, emphasizing the dominance of episodic extreme events (Al-Dousari et al., 2021; Cugerone et al., 2018) and highlighting the limitations of fixed thresholds in dust prone environments (Alexis et al., 2022). Upper tail behaviour corresponded to synoptic dust episodes (Yang et al., 2024). Strong agreement between surface and satellite indicators confirmed the surface atmosphere coupling of dust (Tu et al., 2021), while multi source reanalysis products enhanced reliability in data scarce conditions (Sarafian et al., 2025).

Data-driven thresholds showed lower cutoffs for PM_{10} and AOD_{550} compared with dust indices, reflecting Sanandaj's semi-arid background (Bahadar Zeb et al., 2022; Hamzeh et al., 2021) and the physical selectivity of DOD and $DUAOD_{550}$ (Mousavi et al., 2024). Consistency between K-Means classification and KDE bimodality confirmed methodological robustness (Zeinali et al., 2023; Nissenbaum et al., 2023). Boolean assessment indicated that while AND logic increases precision, OR logic better captures events and was preferred due to regional priorities, with acceptable sensitivity behaviour and supportive validation against METAR observations (Tong et al., 2022; Xi et al., 2021).

Backward trajectory clustering revealed a dual transport regime (Bayat et al., 2024). Cluster 0 represents long range advection from the Syrian Desert and northern-western Mesopotamia, characterized by longer pathways, elevated and stable air masses, and synoptic scale control. Cluster 1 reflects shorter range regional transport from the Iraq-Iran borderlands and southern Mesopotamia, influenced more strongly by boundary layer dynamics, consistent with associated thermodynamic contrasts (Mashat et al., 2020; Karami et al., 2021; Niu et al., 2023; Ma et al., 2023; Fix et al., 2024; Salmabadi et al., 2025; Fattahi Masrour & Rezazadeh, 2022).

From a management perspective, Cluster 0 implies the need for cross border cooperation, whereas Cluster 1 allows more targeted and timely national action. Overall, the integration of multi-indicator statistics, thresholding, and trajectory clustering forms a coherent and transferable framework for diagnosing dust dynamics, supporting more reliable forecasting, early warning, and mitigation under increasing climatic aridity.

4. Conclusion

This study developed and rigorously validated a reproducible, multi-source, data-driven framework for the objective identification of dusty days in a data scarce region of western Iran during 2003 to 2024. By integrating long-term PM_{10} observations with satellite, and reanalysis aerosol indices (AOD_{550}, DOD, $DUAOD_{550}$), the framework establishes defensible quantitative thresholds that overcome the subjectivity of single indicator or empirically tuned approaches. Independent validation using METAR dust and visibility reports confirms the reliability of the identified events and demonstrates the capability of satellite-based proxies to support long term monitoring where surface observations are sparse. The comparative assessment of Boolean rules further demonstrates methodological flexibility, with OR logic favoring comprehensive climatological detection and AND logic providing higher specificity for health applications.

Building upon these objectively detected events, 72-h HYSPLIT backward trajectories combined with resampling, PCA, and clustering revealed two physically distinct transport regimes: (i) proximal sources linked to the Iraq-Iran borderlands and southern Mesopotamia, and (ii) longer range intrusions from the Syrian Desert and northern-western Mesopotamia. These regimes differ systematically in transport distance, speed, and synoptic context, highlighting the coexistence of rapid regional influences and slower large scale advection, with clear implications for both early warning and transboundary mitigation strategies.

The key advancement of this research is the introduction of a unified and transferable framework that, for the first time, integrates objective multi indicator thresholding, independent validation, and trajectory source attribution within a single consistent structure. While demonstrated for Sanandaj, the approach is broadly applicable to other dust-prone regions with observational constraints and provides a scalable foundation for operational monitoring, risk management, and climate related dust assessments. Future work should extend this framework using higher-resolution datasets and coupled dust-meteorology modeling to further enhance predictive capability.

Glossary

Acronym / Term	Definition
AOD (Aerosol Optical Depth at 550 nm)	Measure of solar radiation extinction by aerosols in the atmospheric column; higher values indicate more dust.
AND Logic	Boolean rule requiring all thresholds (PM_{10}, AOD, DOD, DUAOD) to be exceeded; maximizes specificity.
ARIMA (Autoregressive Integrated Moving Average)	Time-series model combining autoregression, differencing, and moving averages to forecast dust variables.
BSk (Cold Semi-Arid Climate, Köppen classification)	Köppen type with hot, dry summers and cold winters; characteristic of Sanandaj.
BTD (Brightness Temperature Difference)	Thermal infrared channel difference used to detect dust; empirical and region-specific.
CAMS (Copernicus Atmosphere Monitoring Service)	European reanalysis providing global aerosol and meteorological fields; used in dust monitoring.
Cluster 0 (Long-range transport cluster)	Trajectory group with long paths and remote origins (Syrian Desert, western Mesopotamia); ~33% of events.
Cluster 1 (Regional transport cluster)	Trajectory group from nearby sources (Iraq–Iran border, Mesopotamia, Khuzestan); ~67% of events.
CMIP6 (Coupled Model Intercomparison Project Phase 6)	Framework coordinating global climate model experiments.
DOD (Dust Optical Depth)	MERRA-2 parameter representing mineral dust contribution to total AOD.
DS (Dust Storm)	METAR code for intense dust storms with visibility reduction.
DU (Dust)	METAR code for dust in suspension, used for validation.

DUAOD (Dust Absorbing Aerosol Optical Depth at 550 nm)	CAMS product isolating absorbing mineral dust at 550 nm.
dusty_all	Daily label for dust defined by any positive code (DU, DS, SA, or HZ).
dusty_strict	Daily label for dust defined only by DU, DS, or SA codes.
EAC4 (ECMWF Atmospheric Composition Reanalysis 4)	Global reanalysis of atmospheric composition from ECMWF.
ECMWF (European Centre for Medium-Range Weather Forecasts)	European center producing forecasts and reanalysis.
ERA5 (ECMWF Reanalysis v5)	Latest ECMWF reanalysis with hourly global data.
EWS (Early Warning System)	Framework combining ground, satellite, and trajectories for real-time dust alerts.
FLEXPART (Flexible Particle dispersion model)	Lagrangian model for atmospheric transport and source attribution.
HFMETAR (High-Frequency METAR)	Enhanced METAR dataset with 5-min reporting intervals.
HZ (Haze)	METAR code for reduced visibility due to fine particles or moisture.
HYSPLIT (Hybrid Single-Particle Lagrangian Integrated Trajectory model)	NOAA model for transport and dispersion; used for 72-h back-trajectories.
ICAO (International Civil Aviation Organization)	UN agency setting aviation codes, e.g., OICS for Sanandaj.
IEM (Iowa Environmental Mesonet)	U.S. portal providing archived meteorological reports, including METAR.
KDE (Kernel Density Estimation)	Method for estimating probability density; used in thresholds and source mapping.
K-Means Clustering	Unsupervised algorithm partitioning data into K groups.
MADIS (Meteorological Assimilation Data Ingest System)	NOAA system integrating and distributing meteorological observations.
METAR (Meteorological Aerodrome Report)	Coded aviation weather reports with visibility and dust codes.
MERRA-2 (Modern-Era Retrospective Analysis for Research and Applications, Version 2)	NASA reanalysis providing dust parameters (e.g., DOD).
MODIS (Moderate Resolution Imaging Spectroradiometer)	NASA satellite sensor producing aerosol and dust indices (e.g., NDDI).
NDDI (Normalized Difference Dust Index)	MODIS spectral index for detecting dust outbreaks.
NOAA (National Oceanic and Atmospheric Administration)	U.S. agency providing datasets, reanalysis, and HYSPLIT.
OICS (Sanandaj Airport ICAO code)	Four-letter ICAO code for Sanandaj Airport, source of METAR.
OR Logic	Boolean rule classifying a day as dusty if any threshold is exceeded; maximizes sensitivity.
PCA (Principal Component Analysis)	Method reducing high-dimensional data to main components for clustering.

PM_{10} (Particulate Matter ≤10 μm)	Inhalable particles ≤10 μm; standard air-quality metric and dust indicator.
READY (Real-time Environmental Applications and Display system)	NOAA platform for running HYSPLIT trajectories and accessing meteorology.
SA (Sand)	METAR code for airborne sand, often linked to dust storms.
Silhouette Score	Clustering index (−1 to +1) measuring cohesion and separation.
SP (Surface Pressure)	Atmospheric pressure at the surface (hPa); affects dust mobilization.
SSP245 (Shared Socioeconomic Pathway 2–4.5 $W\ m^{-2}$)	Intermediate scenario with moderate warming (~2.5 °C by 2100).
SSP585 (Shared Socioeconomic Pathway 5–8.5 $W\ m^{-2}$)	High-emission scenario with stronger warming (~4.5 °C by 2100).
T2M (2-meter Air Temperature)	Air temperature at 2 m height (°C).
Trajectory Resampling (12-point method)	Interpolation of 72-h trajectories into 12 uniform points for PCA and clustering.
U10, V10 (10-meter Wind Components)	Zonal (U10) and meridional (V10) winds at 10 m.
UTC (Coordinated Universal Time)	Global time standard for meteorology and aviation.
Watch (Dust Watch)	Alert level triggered by OR logic, signaling possible dust.
Warning (Dust Warning)	Alert level triggered by AND logic, signaling confirmed dust.
WMO (World Meteorological Organization)	UN agency coordinating meteorology, climate, and coding systems.
Z-score Normalization	Method converting variables to zero mean and unit variance.

Declaration of Generative AI and AI-assisted technologies in the writing process

This article was originally written by the authors without the use of any generative AI. The authors employed ChatGPT (GPT-4) solely for proofreading and enhancing the grammar, syntax, and readability of the manuscript. The final text was meticulously reviewed and revised by the authors to ensure accuracy and preserve the original integrity of the work.

Declaration of competing interest

The authors declare that there are no conflicts of interest regarding the publication of this manuscript. No financial, professional, or personal relationships have influenced the research outcomes presented herein.

Funding

This research did not receive any specific grant from funding agencies in the public, commercial, or not-for-profit sectors.

Data availability

The datasets and Jupyter notebooks supporting the findings of this study are publicly available at Zenodo: Hajimirzaei, M. M. (2025). Dataset and Codes for "Unsupervised Clustering for Identifying Dusty Days and Their Sources: A Long-Term Data Study in Sanandaj, Iran" (v1.0) [Data set]. Zenodo. https://doi.org/10.5281/zenodo.17057619

References:

Abadi ARS, Hamzeh NH, Kaskaoutis DG, Opp C, Kazemi AF. (2025). Long-Term Spatio-Temporal Analysis, Distribution, and Trends of Dust Events over Iran. *Atmosphere*. 2025;16(3):334. https://doi.org/10.3390/atmos16030334

Adamkiewicz, Ł., Maciejewska, K., Skotak, K., Krzyzanowski, M., Badyda, A., Juda-Rezler, K., & Dąbrowiecki, P. (2021). Health-Based Approach to Determine Alert and Information Thresholds for Particulate Matter Air Pollution. Sustainability, 13(3), 1345. https://doi.org/10.3390/su13031345

Al-Dousari, N., Ahmed, M., Al-Dousari, A., Al-Daihani, M., & Al-Elaj, M. (2021). Dust particle size and statistical parameters. In A. Al-Dousari (Ed.), *Atlas of fallen dust in Kuwait* (pp. 47–62). Springer. https://doi.org/10.1007/978-3-030-66977-5_3

Alexis, E., Plocoste, T., & Nuiro, S. P. (2022). Analysis of particulate matter (PM_{10}) behavior in the Caribbean area using a coupled SARIMA–GARCH model. *Atmosphere, 13*(6), 862. https://doi.org/10.3390/atmos13060862

Amanollahi, J., Kaboodvandpour, S., Abdullah, A. M., & Ramli, M. F. (2011). Accuracy assessment of moderate resolution imaging spectroradiometer products for dust storms in semiarid environment. *International Journal of Environmental Science & Technology*, *8*(2), 373–380. https://doi.org/10.1007/BF03326224

Bagherabadi, R., & Moeinaddini, M. (2023). Source Tracking of Dust Storms in the west of Iran (Case study: Kermanshah city*). Journal of Desert Management and Agricultural Land (JDMAL), Vol.10,* Article ID: 1973881. https://doi.org/10.22034/JDMAL.2023.1973881.1402

Baghbanan, P., Ghavidel, Y., & Farajzadeh, M. (2020). Temporal long-term variations in the occurrence of dust storm days in Iran. *Meteorology and Atmospheric Physics*, *133*(6), 1189–1203. https://doi.org/10.1007/s00703-020-00728-3

Bahadar Zeb, B., Alam, K., Ditta, A., Ullah, S., Ali, H. M., Ibrahim, M., & Salem, M. Z. M. (2022). Variation in coarse particulate matter (PM_{10}) and its characterization at multiple locations in the semiarid region. *Frontiers in Environmental Science*, *10*, 843582. https://doi.org/10.3389/fenvs.2022.843582

Bakouch, H.S., Cadena, M., & Chesneau, C. (2020) A new class of skew distributions with climate data analysis. *Journal of Applied Statistics*, 48(16), 3002-3024. https://doi.org/10.1080/02664763.2020.1791804

Barati, G. R., Akbariazirani, T., Moradi, M., & Shamekhi, A. (2020). Identification of the synoptic patterns of dust storms over southern provinces of Iran. *Desert*, 25(2), 249–258. https://doi.org/10.22059/JDESERT.2020.79562

Bartoletti, S., & Loperfido, N. (2009). Modelling air pollution data by the skew-normal distribution. *Stochastic Environmental Research and Risk Assessment*, *24*(4), 513–517. https://doi.org/10.1007/s00477-009-0341-z

Bayat, F., Taheri, A., & Panahifar, H. (2024). Quantification of a long-range transport dust event in the Middle East. *E3S Web of Conferences*, *575*, 02001. EDP Sciences. https://doi.org/10.1051/e3sconf/202457502001

Beyranvand, A., Azizi, G., & Alizadeh, O. (2023). Dust in Western Iran: The emergence of new sources in response to shrinking water bodies. *Scientific Reports*, *13*(1), Article 16158. https://doi.org/10.1038/s41598-023-42173-3

Borna, E., Kiani Sadr, M., & Hosseini, S. A. (2021). Linking ground-satellite observations with HYSPLIT Back trajectory modeling to identify dust sources affecting Western Iran: A case study in Lorestan province. *Environmental Health Engineering and Management Journal*, 8(2), 77-86. https://doi.org/10.34172/EHEM.2021.11

Buchard, V., da Silva, A. M., Colarco, P. R., Darmenov, A., Randles, C. A., Govindaraju, R., ... & Ferrare, R. (2017). The MERRA-2 aerosol reanalysis, 1980 onward. *Part II: Evaluation and case studies*. *Journal of Climate*, 30(17), 6851–6872. https://doi.org/10.1175/JCLI-D-16-0613.1

Camuffo, D., della Valle, A., & Becherini, F. (2018). A critical analysis of the definitions of climate and hydrological extreme events. *Quaternary International*, 538, 5-13. https://doi.org/10.1016/j.quaint.2018.10.008

Cugerone, K., De Michele, C., Ghezzi, A., Gianelle, V., & Gilardoni, S. (2018). On the functional form of particle number size distributions: Influence of particle source and meteorological variables. *Atmospheric Chemistry and Physics*, *18*(7), 4831–4842. https://doi.org/10.5194/acp-18-4831-2018

Ebrahimi, S. J., Ebrahimzadeh, L., Eslami, A., & Bidarpoor, F. (2014). Effects of dust storm events on emergency admissions for cardiovascular and respiratory diseases in Sanandaj, Iran. *Journal of environmental health science & engineering*, *12*, 110. https://doi.org/10.1186/s40201-014-0110-x

Fan H, Zhao C, Yang Y and Yang X (2021) Spatio-Temporal Variations of the PM2.5/PM10 Ratios and Its Application to Air Pollution Type Classification in China. *Frontiers in Environmental Science* 9:692440. https://doi.org/10.3389/fenvs.2021.692440

Fattahi Masrour, P., & Rezazadeh, M. (2022). Spatio-temporal distribution of various types of dust events in the Middle East during the period 1996–2015. *Journal of the Earth and Space Physics*, *47*(4), 231-248. https://doi.org/10.22034/jmas.2022.350322.1177

Fix, F., Mayr, G., Zeileis, A., Stucke, I., & Stauffer, R. (2024). Detection and consequences of atmospheric deserts: Insights from a case study. *Weather and Climate Dynamics*, *5*(6), 1545–1560. https://doi.org/10.5194/wcd-5-1545-2024

Ginoux, P., Prospero, J. M., Gill, T. E., Hsu, N. C., & Zhao, M. (2012). Global-scale attribution of anthropogenic and natural dust sources and their emission rates based on MODIS Deep Blue aerosol products. *Reviews of Geophysics*, 50(3). https://doi.org/10.1029/2012RG000388

Givehchi, R., Arhami, M., Tajrishy, M. (2013). Contribution of the Middle Eastern dust source areas to PM_{10} levels in urban receptors: Case study of Tehran, Iran. *Atmospheric Environment*, *75*, 287-295. https://doi.org/10.1016/j.atmosenv.2013.04.039

Hajimirzaei, M. M. (2025). Dataset and Codes for "Unsupervised Clustering for Identifying Dusty Days and Their Sources: A Long-Term Data Study in Sanandaj, Iran" (v1.0) [Data set]. Zenodo. https://doi.org/10.5281/zenodo.17057619

Hamzeh, N. H., Kaskaoutis, D. G., Rashki, A., & Mohammadpour, K. (2021). Long-term variability of dust events in southwestern Iran and its relationship with the drought. *Atmosphere*, *12*(10), 1350. https://doi.org/10.3390/atmos12101350

Hosseini, G., Teymouri, P., Shahmoradi, B., & Maleki, A. (2015). Determination of the Concentration and Composition of PM10 during the Middle Eastern Dust Storms in Sanandaj, Iran. *Journal of research in health sciences*, *15*(3), 182–188. https://pubmed.ncbi.nlm.nih.gov/26411665/

Inness, A., Ades, M., Agustí-Panareda, A., Barré, J., Benedictow, A., Blechschmidt, A.-M., ... & Suttie, M. (2019). The CAMS reanalysis of atmospheric composition. *Atmospheric Chemistry and Physics*, 19(5), 3515–3556. https://doi.org/10.5194/acp-19-3515-2019

Intergovernmental Panel on Climate Change. (2019). Climate Change and Land: An IPCC special report on climate change, desertification, land degradation, sustainable land management, food security, and greenhouse gas fluxes in terrestrial ecosystems. Geneva, Switzerland: IPCC. Retrieved from https://www.ipcc.ch/srccl/

Iraji, F., Memarian, M. H., Joghataei, M., & Ghafarian Malamiri, H. R. (2021). Determining the source of dust storms with use of coupling WRF and HYSPLIT models: A case study of Yazd province in central desert of Iran. *Journal of Arid Environments*, 186, 104396. https://doi.org/10.1016/j.dynatmoce.2020.101197

Jain, A. K. (2010). Data clustering: 50 years beyond K-means. *Pattern Recognition Letters*, 31(8), 651–666. https://doi.org/10.1016/j.patrec.2009.09.011

Jolliffe, I. T. (2002). *Principal Component Analysis* (2nd ed.). Springer. https://doi.org/10.1007/b98835

Karami, S., Kaskaoutis, D.G., Kashani, S.S., Rahnama, M., Rashki, A. (2021). Evaluation of Nine Operational Models in Forecasting Different Types of Synoptic Dust Events in the Middle East. *Geosciences*. 2021; 11(11):458. https://doi.org/10.3390/geosciences11110458

Kaskaoutis, D. G., Kambezidis, H. D., Nastos, P. T., & Kosmopoulos, P. G. (2008). Study on an intense dust storm over Greece. Atmospheric Environment, 42(28), 6884–6894. https://doi.org/10.1016/j.atmosenv.2008.05.017

Kutiel, H. (2003). Dust Storms in the Middle East: Sources of Origin and Their Temporal Characteristics. *Indoor and Built Environment*, 12(6), 419–426. https://doi.org/10.1177/1420326X03037110

Labban, A. H., & Butt, M. J. (2023). Evaluation of MERRA-2 data for aerosols patterns over the Kingdom of Saudi Arabia. *Heliyon*, 9(3), e17047. https://doi.org/10.1016/j.heliyon.2023.e17047

Lian, S., Zhou, L., Murphy, D. M., Froyd, K. D., Toon, O. B., & Yu, P. (2022). Global distribution of Asian, Middle Eastern, and North African dust simulated by CESM1/CARMA. *Atmospheric Chemistry and Physics*, *22*(21), 13659–13676. https://doi.org/10.5194/acp-22-13659-2022

Liao, D., Peuquet, D. J., Duan, Y., Whitsel, E. A., Dou, J., Smith, R. L., Lin, H.-M., Chen, J.-C., & Heiss, G. (2006). GIS approaches for the estimation of residential-level ambient PM concentrations. *Environmental Health Perspectives*, *114*(9), 1374–1380. https://doi.org/10.1289/ehp.9169

Lin, Y.-P., Chu, H.-J., Wu, C.-F., Chang, T.-K., & Chen, C.-Y. (2011). Hotspot analysis of spatial environmental pollutants using kernel density estimation and geostatistical techniques. *International Journal of Environmental Research and Public Health*, *8*(1), 75–88. https://doi.org/10.3390/ijerph8010075

Ma, X., Gao, Q., Jiang, X., Chen, S., Gan, Y., Zhang, T., et al. (2023). Direct effects of air humidity on dust aerosol production: Evidences for the surprising role of electrostatic forces. Geophysical Research Letters, 50, e2023GL103639. https://doi.org/10.1029/2023GL103639

Mashat, A., Awad, A. M., Assiri, M. A., & Labban, A. K. (2020). Dynamic and synoptic study of spring dust storms over northern Saudi Arabia. *Theoretical and Applied Climatology*, 140, 867–883. https://doi.org/10.1007/s00704-020-03095-6

Middleton, N., Tozer, P., & Tozer, B. (2019). Sand and dust storms: underrated natural hazards. *Disasters*, *43*(2), 390–409. https://doi.org/10.1111/disa.12320

Miri, A., Maleki, S., & Middleton, N. (2021). An investigation into climatic and terrestrial drivers of dust storms in the Sistan region of Iran in the early twenty-first century. *The Science of the total environment*, *757*, 143952. https://doi.org/10.1016/j.scitotenv.2020.143952

Modarres, R., & Sarhadi, A. (2009). *Rainfall trends analysis of Iran in the last half of the twentieth century*. Journal of Geophysical Research Atmospheres, 114(D3), D03101. https://doi.org/10.1029/2008JD010707

Mohammadpour, K., Sciortino, M., & Kaskaoutis, D. G. (2021). Classification of weather clusters over the Middle East associated with high atmospheric dust-AODs in West Iran. *Atmospheric Research*, 256, 105682. https://doi.org/10.1016/j.atmosres.2021.105682

Moridnejad, A., Karimi, N., & Ariya, P. A. (2015). A new inventory for Middle East dust source points. *Environmental Monitoring and Assessment*, 187(9), 582. https://doi.org/10.1007/s10661-015-4806-x

Mousavi, H., Panahi, D. M., & Kalantari, Z. (2024). Dust and climate interactions in the Middle East: Spatio-temporal analysis of aerosol optical depth and climatic variables. *Science of the Total Environment, 172176.* https://doi.org/10.1016/j.scitotenv.2024.172176

Nissenbaum, D., Sarafian, R., Rudich, Y., & Raveh-Rubin, S. (2023). Six types of dust events in Eastern Mediterranean identified using unsupervised machine-learning classification. *Atmospheric Environment, 119902.* https://doi.org/10.1016/j.atmosenv.2023.119902

Niu, G., Qi, X., Chen, L., Xue, L., Lai, S., Huang, X., Wang, J., Chi, X., Nie, W., Kerminen, V.-M., Petäjä, T., Kulmala, M., & Ding, A. (2023). The variation in the particle number size distribution during the rainfall: Wet scavenging and air mass changing. *Atmospheric Chemistry and Physics*, *23*(13), 7521–7534. https://doi.org/10.5194/acp-23-7521-2023

Nourmoradi, H., Moradnejadi, K., Moghadam, F. M., Khosravi, B., Hemati, L., Khoshniyat, R., & Kazembeigi, F. (2015). The Effect of Dust Storm on the Microbial Quality of Ambient Air in Sanandaj: A City Located in the West of Iran. *Global journal of health science*, *7*(7 Spec No), 114–119. https://doi.org/10.5539/gjhs.v7n7p114

Parajuli, S. P., Jin, Q., & Francis, D. (2022). Editorial: Atmospheric dust: How it affects climate, environment and life on Earth? *Frontiers in Environmental Science*, *10*, 1058052. https://doi.org/10.3389/fenvs.2022.1058052

Papatheodorou, S., & Achilleos, S. (2025). Epidemiological insights into the health impacts of dust storms. *Current Opinion in Environmental Science & Health*, *46*, 100626. https://doi.org/10.1016/j.coesh.2025.100626

Pelz, M.-T., Schartau, M., Somes, C. J., Lampe, V., and Slawig, T. (2023). A diffusion-based kernel density estimator (diffKDE, version 1) with optimal bandwidth approximation for the analysis of data in geoscience and ecological research, *Geosci. Model Dev.*, 16, 6609–6634, https://doi.org/10.5194/gmd-16-6609-2023

Pisoni, E., Albrecht, D., Marab, T. A., Rosati, R., Tarantola, S., & Thunis, P. (2018). Application of uncertainty and sensitivity analysis to the air quality SHERPA modelling tool. *Atmospheric Environment*, 183, 84–93. https://doi.org/10.1016/j.atmosenv.2018.04.006

Randles, C. A., da Silva, A. M., Buchard, V., Kinne, S., Gelaro, R., Rodgers, E., & Witek, M. L. (2017). The MERRA-2 aerosol reanalysis, 1980 onward. Part I: System description and data assimilation. *Journal of Climate*, *30*(17), 6303–6330. https://doi.org/10.1175/JCLI-D-16-0609.1

Rashki, A., Middleton, N., & Goudie, A. (2021). Dust storms in Iran - Distribution, causes, frequencies and impacts. *Aeolian Research*, *48*, 100655. https://doi.org/10.1016/J.AEOLIA.2020.100655

Rousseeuw, P. J. (1987). Silhouettes: a graphical aid to the interpretation and validation of cluster analysis. *Journal of Computational and Applied Mathematics*, 20, 53–65. https://doi.org/10.1016/0377-0427(87)90125-7

Ruckthongsook, W., Tiwari, C., & Oppong, J. R. (2018). Evaluation of threshold selection methods for adaptive kernel density estimation in disease mapping. *International Journal of Health Geographics*, *17*(10). https://doi.org/10.1186/s12942-018-0129-9

Salmabadi, H., Saeedi, M., Roy, A., & Kaskaoutis, D. (2023). Quantifying the contribution of Middle Eastern dust sources to PM_{10} levels in Ahvaz, Southwest Iran. *Atmospheric Research*. https://doi.org/10.1016/j.atmosres.2023.106993

Salmabadi, H., Saeedi, M., Notaro, M., & Roy, A. (2025). Dust transport pathways from the Mesopotamian Marshes. *Aeolian Research*, *73*, 100975. https://doi.org/10.1016/j.aeolia.2025.100975

Sarafian, R., Nathan, S., Nissenbaum, D., Khan, S., & Rudich, Y. (2025). Correction of CAMS PM_{10} reanalysis improves AI-based dust event forecast. *Remote Sensing*, *17*(2), 222. https://doi.org/10.3390/rs17020222

Sari Sarraf, B., Rasouli, A. A., Mohammadi, G. H. H., & Hoseini Sadr, A. (2016). Long-term trends of seasonal dusty day characteristics—West Iran. *Arabian Journal of Geosciences*, *9*(423). https://doi.org/10.1007/s12517-016-2589-1

Scott, D. W. (2015). Multivariate Density Estimation. Wiley Series in Probability and Statistics. https://doi.org/10.1002/9781118575574

Shahabi, H., Safarrad, T., Hashim, M., & Al-Ansari, N. (2023). Satellite–Synoptic Monitoring of Dominant Dust Entering Western Iran. *Journal of Sensors*, 2023, Article ID 3069921. https://doi.org/10.1155/2023/3069921

Shahsavani, A., Tobías, A., Querol, X., Stafoggia, M., Abdolshahnejad, M., Mayvaneh, F., Guo, Y., Hadei, M., Hashemi, S. S., Khosravi, A., Namvar, Z., Yarahmadi, M., & Emam, B. (2020). Short-term effects of particulate matter during desert and non-desert dust days on mortality in Iran. *Environment International*, 134, 105299. https://doi.org/10.1016/j.envint.2019.105299

Sorek-Hamer, M., Cohen, A., Levy, R. C., Ziv, B., & Broday, D. M. (2013). Classification of dust days by satellite remotely sensed aerosol products. *International Journal of Remote Sensing*, 34(8), 2672–2688. https://doi.org/10.1080/01431161.2012.748991

Sotoudeheian, S., Gholami, M., & Mousavi, S. M. (2016). Impact of Middle Eastern dust sources on PM_{10} in Iran: Highlighting the impact of Tigris–Euphrates basin sources and Lake Urmia desiccation. *Journal of Geophysical Research: Atmospheres, 121*(15), 9109–9126. https://doi.org/10.1002/2016JD025119

Statistical Centre of Iran & United Nations ESCAP. (2018). *Iran Population and Housing Census 2016: Selected findings*. Report prepared by the Statistical Centre of Iran, presented at the ESCAP Regional Workshop on the 2020 World Programme on Population and Housing Censuses, Bangkok, 24–26 January 2018. https://www.unescap.org/sites/default/files/Session6_Iran_Population_and_Housing_Census2016_Census_WS_24-26Jan2018.pdf

Stein, A. F., Draxler, R. R., Rolph, G. D., et al. (2015). NOAA's HYSPLIT atmospheric transport and dispersion modeling system. *Bulletin of the American Meteorological Society*, 96(12), 2059–2077. https://doi.org/10.1175/BAMS-D-14-00110.1

Stieb, D. M., Burnett, R. T., Smith-Doiron, M., Brion, O., Shin, H. H., & Economou, V. (2008). A New Multipollutant, No-Threshold Air Quality Health Index Based on Short-Term Associations Observed in Daily Time-Series Analyses. *Journal of the Air & Waste Management Association*, *58*(3), 435–450. https://doi.org/10.3155/1047-3289.58.3.435

Tong, Z., Ma, X., Luo, G., Zheng, S., & Zhu, W. (2022). Detecting and evaluating dust events in North China with ground air quality data. *Earth and Space Science*, *9*(3), e2021EA001849. https://doi.org/10.1029/2021EA001849

Tu, Q., Hao, Z., Yan, Y., Tao, B., Chung, C., & Kim, S. (2021). Aerosol optical properties around the East China Seas based on AERONET measurements. *Atmosphere, 12*(5), 642. https://doi.org/10.3390/atmos12050642

U.S. Environmental Protection Agency. (2012). The national ambient air quality standards for particle pollution. EPA. https://www.epa.gov/criteria-air-pollutants/naaqs-table

United Nations Environment Programme. (2016). Global assessment of sand and dust storms. UNEP, WMO, UNCCD. https://wesr.unep.org/media/docs/assessments/global_assessment_of_sand_and_dust_stormsx.pdf

White, J. R., Balling, R. C., & Cerveny, R. S. (2023). Trajectory analysis of central Sonoran Desert dust storms. *Journal of Arid Environments, 219*, Article 105077. https://doi.org/10.1016/j.jaridenv.2023.105077

World Bank. (2019). Sand and Dust Storms in the Middle East and North Africa (MENA) Region: Sources, Costs and Solutions. Washington, DC: World Bank. Retrieved from https://documents1.worldbank.org/curated/en/483941576489819272/pdf/SAND-AND-DUST-STORMS-IN-THE-MIDDLE-EAST-AND-NORTH-AFRICA-MENA-REGION-SOURCES-COSTS-AND-SOLUTIONS.pdf

World Health Organization. (2021). WHO global air quality guidelines: Particulate matter ($PM_{2.5}$ and PM_{10}), ozone, nitrogen dioxide, sulfur dioxide and carbon monoxide. WHO. https://www.who.int/publications/i/item/9789240034228

World Meteorological Organization. (2019). Manual on Codes – Volume I.2: WMO-306 (2019 edition). Geneva, Switzerland: WMO. Retrieved from https://library.wmo.int/index.php?lvl=notice_display&id=20782

Xi, B., Lin, C., & Chen, P. F. (2021). Revisiting the recent dust trends and climate drivers using horizontal visibility and present weather observations. *Journal of Geophysical Research: Atmospheres*, *126*(22), e2021JD034687. https://doi.org/10.1029/2021JD034687

Yang, L., She, L., Che, Y., He, X., Yang, C., & Feng, Z. (2023). Analysis of Dust Detection Algorithms Based on FY-4A Satellite Data. *Applied Sciences*, 13(3), 1365. https://doi.org/10.3390/app13031365

Yang, Q., Yuan, Q., Yue, L., Li, T., Shen, H., & Zhang, L. (2019). The relationships between PM2.5 and AOD in China: About and behind spatiotemporal variations. *Environmental Pollution*, 248, 526-535. https://doi.org/10.1016/j.envpol.2019.02.071

Yang, X., Peng, J., Liu, B., & Liu, Y. (2024). Multi-scale analysis of grain size in the component structures of sediments accumulated along the desert–loess transition zone of the Tengger Desert and implications for sources and aeolian dust transportation. *Atmosphere*, *15*(2), 239. https://doi.org/10.3390/atmos15020239

Zeinali, B., Juq, F. V. G., Teymouri, M., & others. (2023). Selection of the best clustering technique in order to zone the frequency of dust storms in Iran. *Arabian Journal of Geosciences*, *16*, 74. https://doi.org/10.1007/s12517-022-11135-w